Article

Structural basis of salicylic acid perception by *Arabidopsis* NPR proteins

https://doi.org/10.1038/s41586-020-2596-y

Received: 8 August 2019

Accepted: 13 May 2020

Published online: 12 August 2020

Check for updates

Wei Wang[1,2,8], John Withers[3,8], Heng Li[1,5,8], Paul J. Zwack[3], Domnița-Valeria Rusnac[1], Hui Shi[1], Lijing Liu[3,6], Shunping Yan[3,7], Thomas R. Hinds[1], Mikelos Guttman[4], Xinnian Dong[3]✉ & Ning Zheng[1]✉

Salicylic acid (SA) is a plant hormone that is critical for resistance to pathogens[1–3]. The NPR proteins have previously been identified as SA receptors[4–10], although how they perceive SA and coordinate hormonal signalling remain unknown. Here we report the mapping of the SA-binding core of *Arabidopsis thaliana* NPR4 and its ligand-bound crystal structure. The SA-binding core domain of NPR4 refolded with SA adopts an α-helical fold that completely buries SA in its hydrophobic core. The lack of a ligand-entry pathway suggests that SA binding involves a major conformational remodelling of the SA-binding core of NPR4, which we validated using hydrogen–deuterium-exchange mass spectrometry analysis of the full-length protein and through SA-induced disruption of interactions between NPR1 and NPR4. We show that, despite the two proteins sharing nearly identical hormone-binding residues, NPR1 displays minimal SA-binding activity compared to NPR4. We further identify two surface residues of the SA-binding core, the mutation of which can alter the SA-binding ability of NPR4 and its interaction with NPR1. We also demonstrate that expressing a variant of NPR4 that is hypersensitive to SA could enhance SA-mediated basal immunity without compromising effector-triggered immunity, because the ability of this variant to re-associate with NPR1 at high levels of SA remains intact. By revealing the structural mechanisms of SA perception by NPR proteins, our work paves the way for future investigation of the specific roles of these proteins in SA signalling and their potential for engineering plant immunity.

SA is a pivotal defence hormone in plants that accumulates upon pathogen invasion to trigger systemic acquired resistance[1–3]. Previous genetic studies of SA-insensitive mutants in *A. thaliana* have identified *NONEXPRESSOR OF PATHOGENESIS-RELATED GENES 1* (*NPR1*) as a transcriptional coactivator that is indispensable for the expression of antimicrobial PATHOGENESIS-RELATED (PR) genes and for broad-spectrum resistance to disease[4,5]. In contrast to NPR1, NPR3 and NPR4 are negative regulators of plant defence; *npr3 npr4* double mutant plants show elevated expression of PR genes, and increased basal resistance[6,7]. On the basis of their high affinities towards SA, NPR3 and NPR4 have previously been established as SA receptors[7,8]. NPR1 has also been reported to bind SA, although the activity seems to vary in different studies[8–10]. NPR proteins share an N-terminal domain known as the broad-complex, tram track and bric-a-brac (BTB) or poxvirus, zinc finger (POZ) domain, which is commonly found in the substrate receptor subunits of the CULLIN3–RBX1 ubiquitin ligase complexes (CRL3s)[11]. Consistent with their negative role in SA signalling, NPR3 and NPR4 act as CRL3 substrate receptors for NPR1 polyubiquitination and degradation[7,12]. Because their interactions with NPR1 are sensitive to SA, NPR3 and NPR4 regulate SA-mediated gene expression by controlling the stability of NPR1[7,13]. A recent study has suggested that NPR3 and NPR4 might also function independently of NPR1, acting as transcriptional co-repressors with activities that are blocked by SA[8]. A better understanding of how NPR proteins regulate plant immunity in response to SA calls for detailed analysis of the relationships between structure and function in these proteins.

Mapping the SA-binding core domain

Besides the N-terminal BTB domain, all NPR proteins share a central ankyrin repeat (ANK) domain and a C-terminal domain[4,14] (Fig. 1a). Despite extensive efforts, determination of the structure of full-length NPR proteins has been hampered by the poor resolution of single-crystal X-ray diffraction. To overcome this problem, we performed limited proteolytic digestion of different NPR4 constructs to map the minimal SA-binding core (SBC) that is responsible for the SA-sensitive digestion pattern. We identified amino acids 373 to 516 within the NPR4 C-terminal domain as the SBC (Fig. 1a, b, Extended Data Fig. 1a–f, Supplementary Discussion). Using hydrogen–deuterium-exchange mass spectrometry (HDX-MS) of the full-length protein, we confirmed

[1]Department of Pharmacology, Howard Hughes Medical Institute, University of Washington, Seattle, WA, USA. [2]State Key Laboratory of Crop Stress Adaptation and Improvement, School of Life Sciences, Henan University, Kaifeng, China. [3]Department of Biology, Howard Hughes Medical Institute, Duke University, Durham, NC, USA. [4]Department of Medicinal Chemistry, University of Washington, Seattle, WA, USA. [5]Present address: Kronos Bio, Inc., Cambridge, MA, USA. [6]Present address: Key Laboratory of Plant Development and Environment Adaptation Biology, Ministry of Education, School of Life Sciences, Shandong University, Qingdao, China. [7]Present address: College of Life Science and Technology, Huazhong Agricultural University, Wuhan, China. [8]These authors contributed equally: Wei Wang, John Withers, Heng Li. ✉e-mail: xdong@duke.edu; nzheng@uw.edu

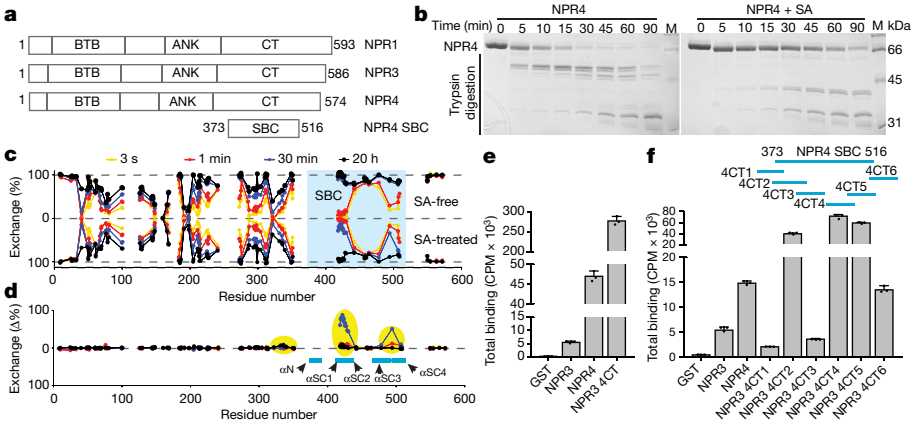

Fig. 1 | Mapping the NPR4 core domain that binds SA. a, Domain arrangements of *A. thaliana* NPR1, NPR3 and NPR4. CT, C-terminal domain. **b**, Trypsin digestion profiles of full-length NPR4 with or without 1 mM SA. M, molecular mass marker. **c**, Mirror plots showing the percentage of deuterium exchange after 3 s (yellow), 1 min (red), 30 min (blue) and 20 h (black) for each observable peptide at the midpoint of their primary sequence for the apo (top) and SA-bound (bottom) NPR4, with SBC region highlighted in light blue. **d**, Net difference (SA-free − SA-treated) in the percentage of deuterium exchange at each time point plotted for each observable peptide. Regions with slowed exchange upon SA binding fall in the positive *y*-axis, and are highlighted in yellow. Broken lines indicate gaps in the sequence coverage. Blue bars and arrows indicate SBC secondary structure elements. **e**, **f**, SA binding by NPR3, NPR4 and NPR3–NPR4 chimeric proteins in the presence of 200 nM (**e**) and 100 nM (**f**) ^{3}H-SA. Horizontal blue lines above the bar graph in **f** indicate the NPR4 regions swapped into NPR3 in comparison to NPR4 SBC. CPM, counts per minute. GST, glutathione *S*-transferase. NPR4 regions: 4CT (residues 345–574); 4CT1 (residues 345–394), 4CT2 (residues 369–428), 4CT3 (residues 395–444), 4CT4 (residues 445–494), 4CT5 (residues 469–518) and 4CT6 (residues 495–574). $n = 3$ independent samples.

that the SBC is the predominant region of NPR4 that has a deuterium uptake profile that is sensitive to SA (Fig. 1c, d, Extended Data Fig. 2, Supplementary Table). The critical role of SBC in sensing SA was further manifested by the notable enhancement of SA binding when the C-terminal domain or SBC sequences of NPR4 were used to replace the corresponding regions of NPR3 (Fig. 1e, f). Although the isolated SBC of NPR4 was mostly insoluble when overexpressed in *Escherichia coli*, we were able to purify the fragment under denaturing conditions and refold the polypeptide in the presence of SA (Extended Data Fig. 1g–i). We subsequently crystallized the SBC of NPR4 and determined its structure at 2.3 Å resolution (Extended Data Table 1).

Crystal structure of SA-bound NPR4 SBC

The structure of the SBC of NPR4 consists of five closely packed α-helices, and the C-terminal four-helix-bundle-like fold contains the SA-binding site (Fig. 2a). We named the four helices that contact SA as αSC1, αSC2, αSC3 and αSC4. These four helices resemble two interlocked 'V' shapes with SA sequestered between them. Their assembly is further stabilized by the N-terminal α-helix (designated αN) on the side. Notably, the electron density is missing for the entire loop that links αSC2 and αSC3, which is presumably disordered in the crystal—a feature that is consistent with its rapid deuterium exchange in solution independent of SA (Figs. 1c, d, 2a, Extended Data Fig. 2b). This flexible loop includes the VDLNETP sequence (Extended Data Fig. 3a), which has previously been suggested as a putative ethylene-responsive element-binding-factor-associated amphipathic repression (EAR) motif that mediates the repressor function of NPR4[8].

The SA-binding site is located at the tapered end of the four-helix bundle of the SBC of NPR4 and enclosed by residues from all four of αSCs (Fig. 2a), which recognize the hormone from all angles. The bottom of the SA-binding pocket is formed by Glu430 of αSC2 and Cys499 of αSC4, which are supported by two opposing phenylalanine residues, Phe427 and Phe496, from αSC1 and αSC3, respectively (Fig. 2b, c, Extended Data Fig. 3b, c). With the carboxyl group of the Glu430 side chain pointing towards the solvent, these four residues construct a hydrophobic environment that accommodates the benzene moiety of SA. In the middle layer, the planar aromatic ring of the hormone is sandwiched by two small NPR4 residues, Ala423 of αSC1 and Gly492 of αSC3, and its edges are surrounded by four additional hydrophobic residues: Ala431 and Ala434 of αSC2, and Tyr500 and Leu503 of αSC4. By crossing each other right above the hormone, αSC1 and αSC3 seal the SA-binding pocket at the top with two face-to-face valine residues, Val420 and Val489 (Fig. 2a–c). They are joined on the side by Arg419 and Thr488, which introduce polar groups to the SA-binding site. As the hallmark residue of the SA-binding pocket, Arg419 neutralizes the carboxyl group of the hormone with a salt bridge and a hydrogen bond (Fig. 2b, Extended Data Fig. 3b, c). As a whole, the SA-binding pocket is characterized by its central location within the receptor SBC domain and its overall hydrophobicity, which are two properties shared by the high-affinity SA-binding pocket of the methyl-SA esterase SABP2[15], and a strategically situated arginine residue. The SA-binding pocket completely buries the hormone inside an internal cavity at the tapered end of the four-helix-bundle-like fold, leaving no gap for the ligand to enter or escape (Fig. 2c, Extended Data Fig. 3d). This precise location of the SA-binding site is supported by the fact that it is strongly protected by SA against deuterium exchange (Fig. 2d). To reconcile the ability of SA to access this site in the full-length protein as detected by HDX-MS (Fig. 1c, d), we postulate that the crystal structure has captured the closed SA-bound conformation of NPR4 SBC, which is stabilized by crystal packing in the absence of the rest of the protein.

To validate the structure in the context of the full-length NPR4 protein, we purified a series of NPR4 mutants with the SA-contacting residues individually mutated. As expected, the majority of these mutants lost SA-binding activity (Fig. 2e). Importantly, NPR4 could not tolerate a change at Arg419 (R419K, R419Q or R419A) (Fig. 2e) nor could NPR3 at Arg428 (Extended Data Fig. 3e), which underscores the critical role of the residue in binding SA. In fact, missense mutation of this arginine confers an SA-insensitive phenotype to the *Arabidopsis npr4-4D* mutant[8]. One of the few outliers amongst the mutants in terms of losing SA-binding activity (NPR4(A434V)) can be rationalized by its nearby empty space in the SA-binding pocket, the size of which also potentially explains the affinity of the SA receptor towards the bulkier SA analogue, benzothiadiazole (Extended Data Fig. 3d). Thr488 probably contributes to SA binding by van der Waals packing, despite its close proximity (3.7 Å) to the 2-hydroxyl group of SA (Fig. 2b). NPR4(T488A)

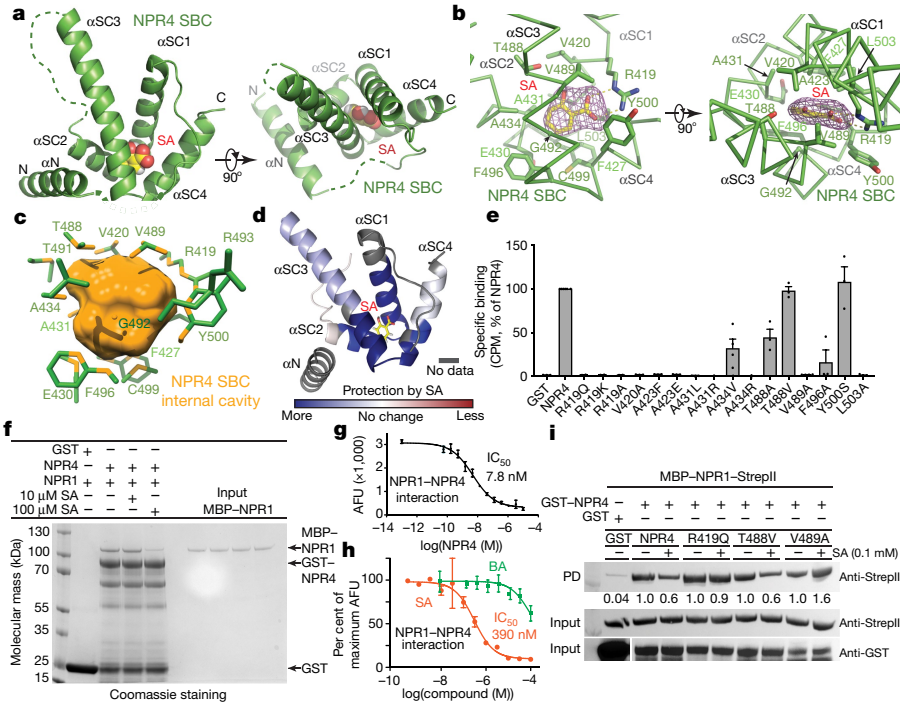

Fig. 2 | Crystal structure of the SA-bound NPR4 SBC. a, Overall views of the SA-bound NPR4 SBC structure with NPR4 in green, SA in space-filling model and secondary structural elements labelled. Dashed lines represent disordered regions. C, C terminus; N, N terminus. **b**, Close-up views of NPR4 SBC bound to SA (yellow and red stick) with its positive $F_o - F_c$ electron density contoured at 4σ (purple mesh). Residues that contact SA are shown in stick model, and polar interactions are represented by yellow dashes. **c**, A close-up view of the NPR4 SBC internal cavity (orange) with SA completely buried inside. Residues of NPR4 that contact SA are shown in stick (green), and their atoms that form the internal cavity surface are coloured in orange. **d**, Structural mapping of SA-induced differences in HDX of NPR4-SBC-sequence regions at the 30-min time point. Regions in blue are protected upon SA (yellow and red sticks) binding. **e**, SA-binding activities of wild-type and mutant NPR4 at 500 nM ^{3}H-SA. $n = 3$ independent samples. **f**, In vitro pulldown of MBP–NPR1–StrepII by GST–NPR4 under two concentrations of SA. Protein interactions were assessed by SDS–PAGE, followed by Coomassie staining. **g**, **h**, AlphaScreen competition and titration assays assessing the NPR1–NPR4 binding affinity with the half-maximal inhibitory concentration (IC_{50}) value indicated (**g**) and the potency of SA in disrupting NPR1–NPR4 binding, with benzoic acid (BA) as a negative control (**h**). $n = 3$ independent samples. AFU, arbitrary fluorescence units. **i**, In vitro pulldown (PD) of MBP–NPR1–StrepII with GST–NPR4 point mutants in the absence or presence of 0.1 mM SA. Protein interactions were assessed by western blot using GST (anti-GST) and StrepII (anti-StrepII) antibodies. Numbers below each sample are ratios that indicate NPR1 levels (+SA) compared to the controls (−SA).

showed a reduction in SA binding, whereas the T488V substitution had little effect (Fig. 2e).

Disruption of NPR1–NPR4 interaction by SA

The lack of any ligand-entry pathway in the structure of the NPR4 SBC–SA complex indicates that the apo form of the receptor must adopt a different conformation, in which its ligand-binding site is accessible to free SA. Such an obligated structural rearrangement of the NPR4 SBC by SA is corroborated by the prominent SA-triggered changes of the deuterium exchange rate of this SBC (Fig. 1d). To investigate the functional consequences of NPR4 SBC remodelling by SA, we first validated NPR1–NPR4 binding in a glutathione *S*-transferase pull-down assay and quantified the interaction in an AlphaScreen-based competition assay, which revealed a strong affinity between the two proteins (Fig. 2f, g). In a dose-dependent manner, SA—but not the inactive benzoic acid—can block the NPR1–NPR4 interaction with potency of about 390 nM (Fig. 2h). We subsequently prepared three representative NPR4 mutants (NPR4(R419Q), NPR4(T488V) and NPR4(V489A)), all of which interacted with NPR1 in the absence of SA (Fig. 2i). As expected, SA was able to weaken the interaction between NPR1 and NPR4(T488V), which retains intact SA-binding activity (Fig. 2e, i). By contrast, the disruptive effect of SA was diminished in NPR4(R419Q) and NPR4(V489A), which are defective in SA binding. These results support the notion that SA is able to regulate NPR4–NPR1 interaction by inducing conformational changes in the NPR4 SBC.

SA-binding activity of NPR1

Arabidopsis NPR4 and NPR1 share 38.1% sequence identity in their SBC regions (Extended Data Fig. 4a). On the basis of sequence alignment, all 14 amino acids that outline the NPR4 SA-binding pocket are highly conserved between NPR4 and NPR1 orthologues and paralogues (Extended Data Fig. 3a). Notably, missense mutations of four of these residues have previously been identified in *Arabidopsis npr1* alleles that are insensitive to benzothiadiazole[16]. The SA-insensitive phenotype of the *Arabidopsis nim1-4* mutant has also previously been attributed to a missense mutation of an NPR1 arginine residue (Arg432)[5], which is equivalent to Arg419 of NPR4. Combined with our structure data, these lines of genetic and bioinformatic evidence suggest that NPR1 and NPR4 share the ability to recognise SA, as well as the structural mechanism of SA recognition.

To re-evaluate SA binding by NPR1, we adopted a recently published procedure[8,10] and established a dose–response curve for SA binding by NPR1 tagged with maltose-binding protein (MBP–NPR1) (Extended Data Fig. 4b, c). The SA-binding signals in these experiments were markedly weaker than those of NPR4. On the basis of the experimental conditions, we estimated that less than 0.02% of the total MBP–NPR1 in the sample was competent for binding the hormone (Fig. 3a). By contrast, about 8% of NPR4 was occupied by SA at the same saturating concentration. Similar to NPR4, the isolated SBC fragment of NPR1 was insoluble when overexpressed in *E. coli*. Upon co-expression, we were able to co-purify soluble NPR1 SBC with NIMIN2 (Fig. 3b)—a protein that has previously been identified to bind NPR1[17,18]—and detect

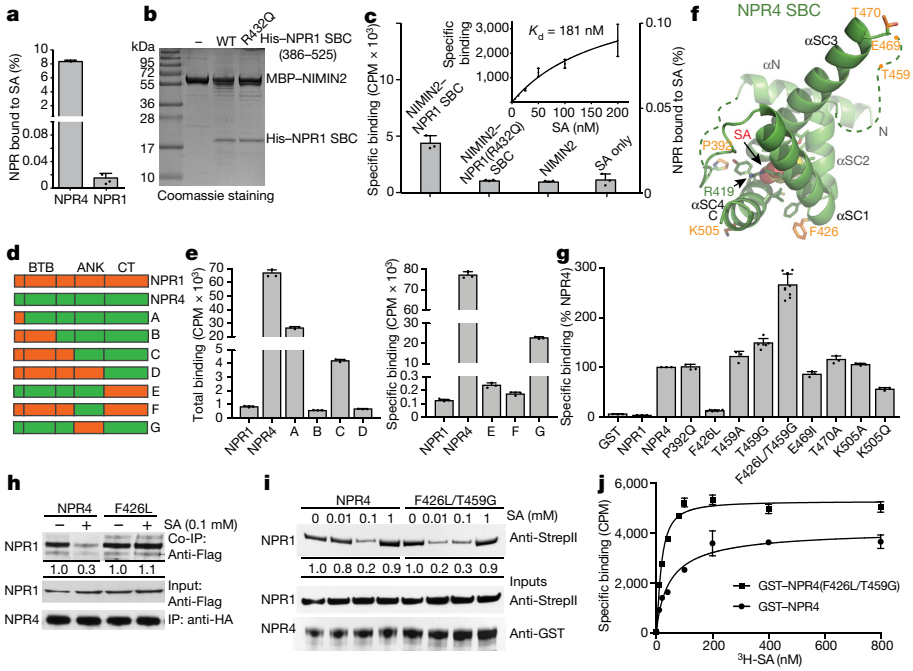

Fig. 3 | Differential SA binding by NPR1 and NPR4 proteins. a, A comparison of SA binding-site occupancy of His–MBP–NPR1 and GST–NPR4 at 800 nM ^{3}H-SA. **b**, Copurification of His–MBP–NIMIN2 with His–NPR1 SBC or His–NPR1(R432Q) SBC co-expressed in *E. coli*, with His–MBP–NIMIN2 alone as a control. Protein interactions were examined by SDS–PAGE followed by Coomassie staining. WT, wild type. **c**, A comparison of SA-binding activities of MBP–NIMIN2 alone, MBP–NIMIN2-bound NPR1 SBC, and MBP–NIMIN2-bound NPR1(R432Q) SBC, with a SA-only sample indicating the background signal. Inset, a dose–response curve for SA binding to MBP–NIMIN2-bound NPR1 SBC. **d**, Design of NPR1–NPR4 chimeric proteins (labelled A to G). The residues involved in the swaps are shown in Extended Data Fig. 4d. **e**, SA binding by NPR1, NPR4 and NPR1–NPR4 chimeric proteins illustrated in **d**. **f**, Structural positions of NPR4 SBC surface residues (orange sticks) selected for mutational analysis. **g**, SA-binding activities of NPR4 SBC surface-residue mutants at 100 nM ^{3}H-SA. **h**, Co-immunoprecipitation (co-IP) of NPR1–Flag with NPR4–HA or NPR4(F426L)–HA, with ratios indicating NPR1 levels (+SA, 0.1 mM) compared to the controls (−SA). **i**, In vitro pulldown of NPR1 with NPR4 or NPR4(F426L/T459G) with the ratios of NPR1 compared to 0 mM SA listed below. **j**, Saturation binding analysis of GST–NPR4 (K_d 49.9 ± 9.2 nM; h, 0.9; R^2 0.96) and GST–NPR4(F426L/T459G) (K_d 17.2 ± 2.5 nM; h 1.3; R^2 0.98). n = 3 independent samples for all statistical data.

an Arg432-dependent SA binding activity in the presence of NIMIN2 (Fig. 3c). Thus, the SA-binding region of NPR1 can be mapped to its SBC, despite the absence of a cysteine residue (Cys529) that has previously been reported to be necessary for hormone binding[9]. Similar to the full-length protein, the predominant population of the NIMIN2-bound NPR1 SBC fragment was dormant in the binding assay. Together, these results confirmed that NPR1 is equipped with an SBC module that is capable of sensing SA. However, NPR1 and NPR4 are categorically distinct from each other by the disparity of their SA-binding activities.

SBC surface residues that affect SA binding

To map the sequence determinants of differential SA binding in NPR1 and NPR4, we performed domain-swapping experiments, which indicated that the NPR4 C-terminal domain or the structurally defined SBC domain is not the only region that contributes to strong SA-binding activity (Fig. 3d, e, Extended Data Fig. 4d). Regions that are N-terminal to SBC, such as the ANK and BTB domains, can effectively alter the ligand-binding activity of SBC in the context of the full-length NPR proteins, presumably through surface residues of the SBC. Consistent with this idea, our HDX-MS analysis revealed small, but detectable, SA-induced structural changes in two overlapping ANK-domain peptides that precede the αN of the SBC (Fig. 1d, Extended Data Fig. 2a). Supporting a role of the surface residues of the SBC in affecting SA binding, replacing the NPR3 C-terminal domain with that of NPR4 conferred an SA-binding activity that is higher than either NPR3 or NPR4 alone (Fig. 1e). To identify the surface residues responsible for this activity, we performed phylogenetic analysis of the C-terminal sequences of angiosperm NPR proteins, and found that these sequences belong to two distinct clades (one similar to *Arabidopsis* NPR1 and NPR2, and the other similar to *Arabidopsis* NPR3 and NPR4) (Extended Data Fig. 5). We selected six clade-specific surface residues for mutagenesis and SA-binding analyses (Fig. 3f, g, Extended Data Fig. 3a).

Among the three mutants with reduced SA binding (NPR4(F426L), NPR4(E469I) and NPR4(K505Q)), we found that the F426L substitution had the strongest effect in reducing SA binding (Fig. 3g). As a solvent-exposed residue on αSC1 (Fig. 3f), F426 is most probably involved in an interdomain interaction that affects ligand binding. Similar to NPR4(R419Q) (Fig. 2i), in vitro-synthesized haemagglutinin (HA)-tagged NPR4(F426L) maintained interaction with Flag-tagged NPR1 in the presence of SA (Fig. 3h). By contrast, mutations of T459 (NPR4(T459A) and NPR4(T459G))—which is located in the middle of the disordered αSC2–αSC3 linker (Fig. 3f)—increased SA binding to NPR4 by up to 50% (Fig. 3g). When the T459G substitution was combined with F426L, the ability of NPR4 to bind SA was markedly enhanced (by about threefold). Consistent with its augmented SA-binding activity, we found that the interaction between NPR4(F426L/T459G) and NPR1 was disrupted by 0.01 mM SA—which is 10 times lower than the concentration required to interfere with interaction between wild-type NPR4 and NPR1 (Fig. 3i). We speculate that these two mutations might have epistatically changed the conformational dynamic of NPR4, which could affect the transition between the apo and SA-bound forms of the receptor. Our saturation binding analyses revealed that NPR4(F426L/T459G) (K_d = 17.2 ± 2.5 nM, h = 1.3) has a higher affinity and binds SA more efficiently than NPR4 (K_d = 49.9 ± 9.2 nM, h = 0.9) (Fig. 3j).

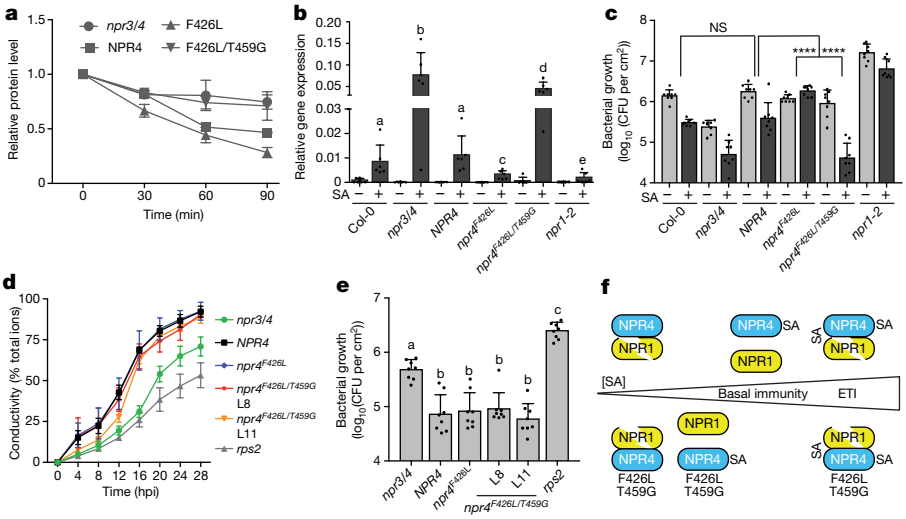

Fig. 4 | Functional effects of two surface-residue mutations in the NPR4 SBC. a, Cell-free protein degradation assays comparing the degradation rates of endogenous NPR1 in *npr3 npr4* (*npr3/4*) lines that express similar amounts of NPR4, NPR4(F426L) or NPR4(F426L/T459G). The samples were pretreated with 0.1 mM SA for 24 h before extraction. The data are mean ± s.e.m. ($n = 3$) of the relative band intensities quantified from western blots (Extended Data Fig. 6b). **b**, *PR1* expression 24 h after mock (−) or 0.1 mM SA (+) treatments. The data are normalized to *UBQ5* expression. $n = 6$ biologically independent samples. Statistical significance was determined by one-way analysis of variance (ANOVA) on log-transformed data, followed by Tukey's multiple comparison correction; letters indicate statistical significance ($P < 0.05$). **c**, SA protection against *P. syringae* pv. *maculicola* ES4326 infection. Bacterial growth in infected leaves was recorded 3 days after inoculation of mock-treated (−) or 0.1 mM SA-treated (+) plants. $n = 8$ biologically independent samples. Statistical significance was determined by two-way ANOVA on log-transformed data. NS, $P > 0.9971$, ****$P < 0.0001$. **d**, **e**, Assays for infection with *P. syringae* pv. *maculicola* expressing AvrRpt2. Ion leakage data are normalized to a total ion count recorded 28 h post-inoculation (hpi) (**d**), and colony-forming units (CFU) in infected leaves were determined 24 hpi (**e**). $n = 3$ (**d**) and 8 (**e**) biologically independent samples. Statistical significance was determined by one-way ANOVA on log-transformed data followed by Tukey's multiple comparison correction, letters indicate statistical significance, $P < 0.05$. L8 and L11 denote independent transgenic lines. **f**, The NPR4(F426L/T459G) double substitution enhances SA perception and SA-induced resistance, without compromising effector-triggered immunity (ETI). At higher concentrations of SA, a second SA-binding site might exist to promote the re-association of NPR1 and NPR4.

Characterization of a SA-hypersensitive mutant

Because the functional importance of SA-contacting residues of the SBC is validated by genetic data[4,5,8,16], we sought to determine whether these surface residues of the NPR4 SBC can also affect SA-induced defence in planta. Given that these residues are not conserved between the NPR1 and NPR4 clades (Extended Data Figs. 3a, 5), they are potential candidates for engineering SA receptors with variable activities. In protein degradation assays conducted using *npr3 npr4* transgenic lines that express similar amounts of wild-type and mutant NPR4, endogenous NPR1 was degraded slower in the presence of NPR4(F426L/T459G) but faster with NPR4(F426L), as compared to the wild-type NPR4 (Fig. 4a, Extended Data Fig. 6a–d). These results are in full agreement with the opposite effects of these mutations on SA binding and interactions with NPR1 in vitro (Fig. 3g–i). We then examined the levels of SA-induced expression of the *PR1* gene in these transgenic lines, and found that NPR4 tagged with green fluorescent protein (NPR4–GFP) reduced *PR1* levels in the *npr3 npr4* double mutants to the wild-type level, whereas two independent NPR4(F426L)–GFP lines further diminished in terms of *PR1* induction (Fig. 4b, Extended Data Fig. 6e, f). By contrast, the NPR4(F426L/T459G)–GFP lines showed a fourfold increase in SA-induced expression of *PR1*, as compared to NPR4–GFP (Fig. 4b, Extended Data Fig. 6g, h). In the subsequent testing of SA-induced disease resistance, we observed that—although the *npr3 npr4* mutants were resistant to infection with *Pseudomonas syringae* pv. *maculicola* ES4326—expression of NPR4, NPR4(F426L) or NPR4(F426L/T459G) all restored the susceptibility to this bacterial pathogen to levels similar to that in Col-0 plants (Fig. 4c). Pre-treatment of plants with 0.1 mM SA produced a significant reduction in bacterial multiplication in the *npr3 npr4* mutants, as well as in the wild-type *NPR4* transgenic lines. This protective effect was lost in the NPR4(F426L) plants but was markedly enhanced in the NPR4(F426L/T459G) plants, as shown by the development of symptoms and by bacterial titre in infected leaves (Fig. 4c, Extended Data Fig. 6i, j). These results clearly demonstrate the opposing biological effects that the F426L and F426L/T459G substitutions in NPR4 had on SA-mediated immunity.

Accumulation of NPR1 in *npr3 npr4* mutant plants enhances basal resistance to *P. syringae* pv. *maculicola*, but compromises effector-triggered immunity to *P. syringae* pv. *maculicola* that express the effector AvrRpt2[7]. When infected with *P. syringae* pv. *maculicola* expressing AvrRpt2, the *npr4*$^{F426L/T459G}$ mutant showed effector-induced cell death (that is, ion leakage) and inhibition of bacterial growth similar to plants with wild-type NPR4 and to the *npr4*^{F426L} mutant (Fig. 4d, e), which suggests that it is possible to enhance SA-mediated resistance without compromising effector-triggered immunity through the engineering of these residues. We rationalize that—despite its enhanced sensitivity to low levels of SA—NPR4(F426L/T459G) can re-associate with NPR1 at high concentrations of SA (similar to wild-type NPR4) through an unknown mechanism (Fig. 3i) to induce NPR1 degradation during effector-triggered immunity (Fig. 4f). Consistent with this, our in planta protein-degradation analysis demonstrates that NPR1 is destabilized in NPR4(F426L/T459G) and NPR4 plants when they are treated with 1 mM SA (Extended Data Fig. 6k). In addition to NPR1, NPR4(F426L/T459G) is most probably able to degrade JAZ proteins, which has previously been shown to be required for effector-triggered immunity[19]. It is also interesting to note that normal effector-triggered immunity is observed for NPR4(F426L). This is consistent with the CRL3 adaptor model, which predicts that the mutant can constitutively remove the inhibition of effector-triggered immunity by NPR1.

Conclusion

This study reveals the structural basis of SA recognition by NPR4 and provides initial insights into the structure–function relationships of

NPR proteins. Future studies will be needed to shed light on the intricate interplay between NPR proteins in SA signalling, and to explore these SA receptors for engineering plant immunity.

Online content

Any methods, additional references, Nature Research reporting summaries, source data, extended data, supplementary information, acknowledgements, peer review information; details of author contributions and competing interests; and statements of data and code availability are available at https://doi.org/10.1038/s41586-020-2596-y.

1. Malamy, J., Carr, J. P., Klessig, D. F. & Raskin, I. Salicylic acid: a likely endogenous signal in the resistance response of tobacco to viral infection. *Science* **250**, 1002–1004 (1990).
2. Métraux, J. P. et al. Increase in salicylic acid at the onset of systemic acquired resistance in cucumber. *Science* **250**, 1004–1006 (1990).
3. Gaffney, T. et al. Requirement of salicylic acid for the induction of systemic acquired resistance. *Science* **261**, 754–756 (1993).
4. Cao, H., Glazebrook, J., Clarke, J. D., Volko, S. & Dong, X. The *Arabidopsis NPR1* gene that controls systemic acquired resistance encodes a novel protein containing ankyrin repeats. *Cell* **88**, 57–63 (1997).
5. Ryals, J. et al. The *Arabidopsis* NIM1 protein shows homology to the mammalian transcription factor inhibitor I kappa B. *Plant Cell* **9**, 425–439 (1997).
6. Zhang, Y. et al. Negative regulation of defense responses in *Arabidopsis* by two *NPR1* paralogs. *Plant J.* **48**, 647–656 (2006).
7. Fu, Z. Q. et al. NPR3 and NPR4 are receptors for the immune signal salicylic acid in plants. *Nature* **486**, 228–232 (2012).
8. Ding, Y. et al. Opposite roles of salicylic acid receptors NPR1 and NPR3/NPR4 in transcriptional regulation of plant immunity. *Cell* **173**, 1454–1467 (2018).
9. Wu, Y. et al. The *Arabidopsis* NPR1 protein is a receptor for the plant defense hormone salicylic acid. *Cell Rep.* **1**, 639–647 (2012).
10. Manohar, M. et al. Identification of multiple salicylic acid-binding proteins using two high throughput screens. *Front. Plant Sci.* **5**, 777 (2015).
11. Genschik, P., Sumara, I. & Lechner, E. The emerging family of CULLIN3–RING ubiquitin ligases (CRL3s): cellular functions and disease implications. *EMBO J.* **32**, 2307–2320 (2013).
12. Spoel, S. H. et al. Proteasome-mediated turnover of the transcription coactivator NPR1 plays dual roles in regulating plant immunity. *Cell* **137**, 860–872 (2009).
13. Castelló, M. J., Medina-Puche, L., Lamilla, J. & Tornero, P. *NPR1* paralogs of *Arabidopsis* and their role in salicylic acid perception. *PLoS ONE* **13**, e0209835 (2018).
14. Rochon, A., Boyle, P., Wignes, T., Fobert, P. R. & Després, C. The coactivator function of *Arabidopsis* NPR1 requires the core of its BTB/POZ domain and the oxidation of C-terminal cysteines. *Plant Cell* **18**, 3670–3685 (2006).
15. Forouhar, F. et al. Structural and biochemical studies identify tobacco SABP2 as a methyl salicylate esterase and implicate it in plant innate immunity. *Proc. Natl Acad. Sci. USA* **102**, 1773–1778 (2005).
16. Canet, J. V., Dobón, A., Roig, A. & Tornero, P. Structure–function analysis of *npr1* alleles in *Arabidopsis* reveals a role for its paralogs in the perception of salicylic acid. *Plant Cell Environ.* **33**, 1911–1922 (2010).
17. Weigel, R. R., Bäuscher, C., Pfitzner, A. J. P. & Pfitzner, U. M. NIMIN-1, NIMIN-2 and NIMIN-3, members of a novel family of proteins from *Arabidopsis* that interact with NPR1/NIM1, a key regulator of systemic acquired resistance in plants. *Plant Mol. Biol.* **46**, 143–160 (2001).
18. Maier, F. et al. NONEXPRESSOR OF PATHOGENESIS-RELATED PROTEINS1 (NPR1) and some NPR1-related proteins are sensitive to salicylic acid. *Mol. Plant Pathol.* **12**, 73–91 (2011).
19. Liu, L. et al. Salicylic acid receptors activate jasmonic acid signalling through a non-canonical pathway to promote effector-triggered immunity. *Nat. Commun.* **7**, 13099 (2016).

Methods

No statistical methods were used to predetermine sample size. The experiments were not randomized and investigators were not blinded to allocation during experiments and outcome assessment.

Molecular cloning

The coding sequences of *A. thaliana NPR1* (AT1G64280), *NPR4* (AT4G19660) and *NIMIN2* (AT3G25882) were amplified by polymerase chain reaction (PCR) from an *Arabidopsis* cDNA library, and sub-cloned into the DH5α strain with different N-terminally fused tags and a tobacco etch virus (TEV)-cleavage site. The specific amino acid changes for the *NPR1* and *NPR4* point mutations were generated using the QuikChange II site-directed mutagenesis kit (Agilent). GST-fused *NPR4* coding sequence (CDS) was subcloned into the pFastBac vector and transformed to *E. coli* DH10Bac for making baculovirus for protein expression in insect cells. Protein domain swaps were generated by amplifying the desired regions of each CDS with primers designed to create overlapping sequences for each fragment. The DNA fragments were amplified in separate PCR reactions, processed with either a PCR clean-up kit or gel extraction kit (Bio Basic), and the desired fragments were fused by PCR using gene-specific forward and reverse primers containing attB1 and attB2 Gateway recombination sequences, respectively. All CDSs were recombined into pDONR207 or pDONR221 and subsequent expression vectors using the Gateway technology and sequenced to confirm accuracy.

Protein purification and preparation

The GST-tagged NPR1, NPR4 and NPR4 fragments were overexpressed in BL21 (DE3) strain. NPR4–GST protein for HDX experiments were expressed in insect cells according to previously described methods[20]. The proteins were purified from the soluble cell lysate by glutathione affinity chromatography. After on-column tag cleavage by TEV protease at 4 °C for 16 h or directly eluted from the affinity column, the proteins were further purified by anion exchange and size-exclusion chromatography. The NPR4 SBC protein was expressed with an N-terminal 6×His tag (His–NPR4 SBC) in BL21 (DE3) cells, first grown to optical density at 600 nm ($OD_{600\,nm}$) of 0.9–1.0 at 37 °C and then induced by 0.5 mM isopropyl-β-D-thiogalactopyranoside (IPTG) at 25 °C overnight. Cells were collected and lysed in extraction buffer (50 mM Tris-HCl, pH 8.0, 500 mM NaCl, 1 mM TCEP) and pellets were collected by centrifugation and resuspended in 50 mM Tris-HCl, pH 8.0, 500 mM NaCl, 8 M urea (denaturation buffer). Denatured His–NPR4 SBC was isolated with Ni-NTA resin and eluted using the denaturation buffer supplemented by 250 mM imidazole before being dialysed against a buffer containing 50 mM Tris-HCl, pH 8.0, 500 mM NaCl, 1 mM DTT and 2 mM SA. His–NPR4 SBC was further purified by anion exchange and gel-filtration chromatography. The peak fractions containing His–NPR4 SBC were collected and concentrated to 15 mg ml^{-1}. A six-amino-acid internal deletion mutant of His NPR4-SBC (NPR4(Δ450–455) SBC) was purified following the same procedure. The His–NPR1–MBP was purified as previously described[8]. To co-purify NPR1 SBC with NIMIN2–MBP, cells co-expressing the two proteins were collected and lysed in 50 mM Tris-HCl, pH 8.0, 150 mM NaCl, 1 mM TCEP. The supernatant was loaded onto an amylose column, which was subsequently washed with the lysis buffer. The protein complexes were eluted using a buffer containing 50 mM Tris-HCl, pH 8.0, 150 mM NaCl, 1 mM TCEP and 10 mM maltose (Supplementary Methods).

Crystallization, data collection and structure determination

The crystals of His–NPR4 SBC protein were grown at 16 °C by the hanging-drop vapour diffusion method with 1 μl protein sample containing 2 mM SA mixed with 1 μl reservoir solution containing 0.25 M potassium phosphate dibasic, 23% PEG 3350, pH 9.2. Large-sized crystals were obtained and collected after 1 week. Twenty per cent glycerol was included in the mother liquor as the cryoprotectant during crystal collection and data collection. To improve the resolution of His–NPR4 SBC crystals, an internal deletion mutant (NPR4(Δ450–455) SBC) was constructed to reduce the length of the disordered loop between αSC2 and αSC3. The heavy-atom derivative crystals were obtained by soaking the native crystals in the presence of 0.1 mM cisplatin (cis $Pt(NH_3)_2Cl_2$) for 6 d. All X-ray diffraction datasets were collected at the Advanced Light Source at Berkeley on beam lines 8.2.1 and 8.2.2. The single anomalous dispersion dataset was collected near the platinum absorption edge ($\lambda = 1.072$ Å). Reflection data were indexed, integrated and scaled with the HKL2000 package[21]. The single anomalous dispersion method was used to determine the initial phase using PHENIX[22] with a 2.8 Å platinum derivative dataset. Initial structural models were built, and refined using COOT[23] and PHENIX. The final model was built and refined with a 2.28 Å native dataset. The final model has 99% of residues in the favoured region and 0% in outliner region of the Ramachandran plot. The asymmetric unit of the crystal contains two copies of NPR4 SBC, the conformation of which might be stabilized by crystal packing.

Trypsin digestion assay

NPR4 constructs of various lengths, or BSA protein, was diluted to 2 mg ml^{-1} using reaction buffer containing 50 mM Tris, pH 8.0, 200 mM NaCl, 1 mM TCEP and incubated with or without 1 mM SA or 3-OH BA for 1 h on ice. Trypsin (Promega) was added to the sample protein at a final concentration of 0.005 mg ml^{-1}. The digestion reaction proceeded for different lengths of time at 20 °C. After the digestion, the samples were analysed by 15% SDS–PAGE and stained with Coomassie blue dye (CBB), then destained in water before imaging.

Tritium-labelled SA-binding assays

All single-concentration SA-binding measurements for GST–NPR4, including all point mutations and chimeric proteins, were conducted as previously described using the ^{3}H-SA concentrations stated in the figure legends[7]. For measuring the SA saturation binding curve of NPR4 and NPR4(F426L/T459G), 2 μg of each protein were bound to 25 μl of magnetic glutathione beads (Pierce) and incubated for 1 h at room temperature with shaking at 1,000 rpm, in 200 μl of sodium citrate buffer pH 6.8 containing the indicated ^{3}H-SA concentrations ranging from 10 to 800 nM. The samples were washed 3 times with 1 ml of binding buffer, resuspended in 100 μl of water, transferred to a scintillation vial and counted with 6 ml of Ultima Gold (Perkin Elmer). For measuring the SA saturation binding curve of the full-length NPR1 and the NPR1 SBC–NIMIN2 complex, ^{3}H-SA (American Radiolabelled Chemicals, 50 Ci/mmole) was mixed with various amounts of cold SA to obtain the required specific activity for each experiment. The binding assay was based on a previously reported procedure with a rapid centrifugation-based gel filtration method[8,10]. Specifically, G-25 QiaShredder mini columns were initially filled with 0.13 g of Sephadex G-25 (fine), which was allowed to swell over night with PBS buffer pH 7.4 containing 0.1% Tween20 in a final volume of about 650 μl. Columns were washed with 1.0 ml buffer by gravity and air pockets were removed before spinning at 1,000*g* for 30 s. The NPR proteins were diluted to between 0.2 and 10 μM. SA was serially diluted to 6.25 nM. The reaction volume was 200 μl and the samples were incubated on ice for 2 h. After incubation, three 50-μl aliquots, each of which is equivalent to 7.7% column volume, were added to the top of the pre-equilibrated G-25 columns without touching the surface. Samples were then immediately centrifuged at 1,000*g* for 2 min. The collected eluate was transferred to a scintillation vial and counted with 5 ml of Ultima Gold (Perkin Elmer). A protein-free SA-only sample was measured using the same procedure as a control for the background signal. For the comparison between NPR1 SBC–NIMIN2 and the NPR1 (R432Q) SBC–NIMIN2 mutant, the SA-only background signal was not subtracted. To estimate the percentage of NPR proteins bound to SA in the ^{3}H-SA binding assay, the concentration of ^{3}H-SA stock solution was first calculated (20 μM) based

on its specific activity (50 Ci/mmol) and radioactivity concentration (1 mCi/ml). By counting a small aliquot of the complete reaction solution with a specific amount of ^{3}H-SA mixed with cold SA at a defined ratio, the number of moles of total SA per CPM was derived. For example, 10 µl of a complete reaction solution with 800 nM total SA prepared by a mixture of ^{3}H-SA and cold SA had 331,686 CPM, which yielded 2.41×10^{-17} moles per CPM. The total number of moles of SA in the gel filtration flow-through fraction for each sample from the SA binding assay was then calculated by multiplying the total CPM by the number of moles of SA per CPM. The concentrations of the purified proteins were determined by the Bradford assay. The amount of the NPR proteins relative to the total proteins was quantified by gel densitometry analysis. The number of moles of the NPR proteins in each SA-binding assay sample was then obtained on the basis of the protein concentration and the reaction volume. The percentage of NPR proteins bound to SA was calculated by dividing the total number of moles of SA by the number of moles of the NPR proteins.

In vitro pulldown assay

The pulldown reactions were conducted as previously described[7] with the following modifications. Each reaction was assembled in 4 ml of buffer with equal amounts (5–10 µg) of protein (GST–NPR4 or GST–NPR4 point mutants) bound to glutathione agarose beads mixed with 50 µg of HIS–MBP–NPR1–StrepII in the presence or absence of sodium salicylate (Na-SA). The reactions were incubated overnight with end-over-end mixing. After incubation, the beads were collected by centrifugation at 700*g* for 1 min and washed 3 times with 0.5 ml of pulldown buffer with or without Na-SA at the appropriate concentration. The samples were resuspended in 50 µl of elution buffer (50 mM Tris-HCl, 200 mM NaCl, 5 mM DTT, 20 mM reduced glutathione, pH 8.0) and incubated at 22 °C with shaking at 900 rpm for 20 min. After centrifugation at 700*g* for 1 min, 50 µl of supernatant for each sample was added to 13 µl of NuPage 4× LDS sample buffer (Life Technologies) containing 200 mM DTT, which was subsequently heated at 95 °C for 10 min. The final samples were resolved by SDS–PAGE and visualized either by staining with the Colloidal Blue Staining Kit (Thermo Fisher Scientific) or by western blot using anti-GST–HRP (GE Healthcare) and anti-StrepII–HRP (Millipore) antibodies. Chemiluminescence was detected using the Super Signal West Pico chemiluminescent substrate (Thermo Fisher Scientific).

HDX-MS assay

Ten microlitres of 0.2 mg ml^{-1} full-length NPR4 protein (incubated with or without 0.1 mM SA) was diluted into 85 µl of D_2O with 5 µl of 20× PBS buffer (with or without 0.1 mM SA) and incubated at room temperature for 3 s, 1 min, 30 min or 20 h. At the desired time point, each sample was rapidly mixed with an equal volume of ice-cold 8 M urea with 0.2% formic acid and 0.1% trifluoroacetic acid (TFA) for a final pH of 2.5 to quench the exchange reaction. The samples were then immediately frozen in liquid nitrogen and stored at −80 °C until liquid chromatography–mass spectrometry (LC–MS) analysis. A fully deuterated sample was prepared by incubating a denatured stock protein in 4 M guanidinium chloride at 85 °C for 10 min, diluting into deuterium as with all other samples, incubating at 60 °C for 2 h, and followed by the same quenching procedure. A 'zero' time point to correct for in-exchange during digestion and sample handling was prepared by pre-mixing the 5 µl of 20× PBS, 85 µl of D_2O and 100 µl of quench before adding the 10 µl of stock protein.

Samples were thawed and injected onto a custom cold box that kept the injection lines and columns at 0 °C. The protein was first passed over a custom-packed 2.1 × 50 mm pepsin column at 200 µl min^{-1} for inline digestion. Peptides were then trapped on a Waters BEH C18 vanguard column (2.1 × 5 mm1.7 µm 130 Å) and resolved over BEH C18 column (1 × 100 mm 1.7 µm 130 Å) using linear gradient of 5 to 35% B (A: 0.1% FA, 0.025% TFA, 5% ACN; B: ACN with 0.1% FA) over 10 min and analysed on a Waters Synapt G2-Si mass spectrometer. A series of washes over the trap and pepsin columns was used between injections to minimize carry-over. An identical liquid chromatography protocol was used with the liquid chromatograph connected to a Thermo LTQ Orbitrap mass spectrometer to collect several rounds of data-dependent acquisition tandem mass spectrometry of an undeuterated samples. Peptides were identified using Protein Prospector with a score threshold of 15.

AlphaScreen competition assay

To monitor NPR1–NPR4 interaction and its disruption by SA, AlphaScreen assays were performed using EnSpire reader (PerkinElmer). MBP-tagged NPR1 was immobilized to anti-MBP AlphaScreen acceptor beads. GST-tagged NPR4 was attached to anti-GST AlphaScreen donor beads. The donor and acceptor beads were brought into proximity by the interactions between NPR1 and NPR4. Competition assays were performed in the presence of tag-free NPR4, SA or BA, all of which were titrated at various concentrations. The experiments were conducted with 10 nM GST–NPR4 and 10 nM MBP–NPR1 in the presence of 10 µg/ml donor and acceptor beads in a buffer of 50 mM Tris-HCl, pH 8.0, 200 mM NaCl, 1 mM TCEP, 0.1% Triton X-100. The experiments were performed in triplicates. IC_{50} values were calculated using nonlinear curve fitting of the dose–response curves generated with Prism 4 (GraphPad).

In vitro translation and co-IP

Epitope-tagged proteins were synthesized using a wheat-germ-based translation system (BioSieg). Synthesized proteins were mixed and incubated with Pierce anti-HA magnetic beads (Thermo Fisher Scientific) overnight at 4 °C in the co-IP buffer (50 mM Tris pH 6.8, 100 mM NaCl, 0.1% nonidet P40 and complete EDTA-free protease inhibitor cocktail (Roche) ± 0.1 mM Na-SA). Following immunoprecipitation, beads were collected and washed 3 times with 1 ml of the pulldown buffer using a magnetic stand, and the samples were eluted by incubation at 95 °C for 10 min in the NuPage LDS sample buffer (Life Technologies), resolved by SDS–PAGE, and visualized by western blot with anti-HA (BioLegend) or anti-Flag (Sigma-Aldrich) antibodies and the Super Signal West Pico chemiluminescent substrate (Thermo Fisher Scientific).

Plant material

The *A. thaliana* genotypes—wild type, *npr1-2* and *npr3-1 npr4-3* (*npr3/4*) double mutant—used in this study were all in the Col-0 background. The CDS of wild-type NPR4 and all point mutants used in this study were recombined into pK7FWG2 to generate C-terminal GFP fusions and transformed into *Arabidopsis npr3 npr4* mutants by floral dip[24]. First-generation transgenic lines were selected on Murashige and Skoog medium supplemented with 50 µg/ml kanamycin and screened by western blot for expression of the GFP fusion proteins. T2 lines containing a single insertion were identified by segregation analysis of the antibiotic resistance in 100 seedlings, and T3 homozygous lines were confirmed by segregation analysis and western blots.

Gene expression analysis

Total RNA was extracted from of plant tissue treated with water or Na-SA using TRIzol reagent (Thermo Fisher Scientific) following the manufacturer's protocol. Total RNA samples were incubated with Turbo DNase (Thermo Fisher Scientific) to ensure removal of any residual DNA. The samples were quantified using a UV5 Nano spectrophotometer (Mettler Toledo) and 2 µg of each was used for cDNA synthesis with Superscript III reverse transcriptase (Thermo Fisher Scientific) following the manufacturer's protocol. cDNA samples were diluted 1:8 in RNase-free water and 2 µl of each was used for quantitative (q)PCR with Fast Start Universal Sybr Green master mix (Roche) using gene-specific primers. qPCR experiments were conducted and analysed using a RealPlex2 Ep-gradient Master Cycler (Eppendorf).

Pathogen infection

Pseudomonas syringae pv. *maculicola* ES4326 or *P. syringae* pv. *maculicola* carrying the effector protein AvrRpt2 were grown at 30 °C on plates containing the King's B medium (KB) for 24 h and resuspended in 10 mM $MgCl_2$. Plants (3.5 weeks old) grown in soil (Metro Mix 200, Grace-Sierra) were used for infection assays. The SA protection assays were conducted as previously described[25]. However, the plants were sprayed with a suboptimal SA concentration (0.1 mM) to demonstrate the enhanced sensitivity of plants expressing NPR4(F426L/T459G). When indicated, bacterial growth from three experiments (eight biological replicates each) were combined using linear mixed effect model (lme4 R package) with experiment as random effects[26]. The ion leakage and bacterial growth experiments using *P. syringae* pv. *maculicola* ES4326 expressing AvrRpt2 were conducted as previously described[19]. All experiments were repeated at least three times with similar results.

Protein degradation assays

Cell-free degradation assays were performed using 12-day-old, liquid-grown seedlings, treated with 0.1 mM Na-SA for 24 h to induce endogenous NPR1 accumulation. The assay was carried out as previously described[27] with the following modifications: To monitor levels of the endogenous NPR1, protein extraction buffer was supplemented with 100 µg/ml cycloheximide to inhibit protein synthesis. Tween-20 (0.05%) was also added to improve recovery of nuclear NPR1. Proteasome inhibitors (MG115 and MG132) were used at a final concentration of 417 µM. Incubations were carried out in the presence of 0.1 mM SA. The samples were resolved by SDS–PAGE and visualized by western blot with an anti-NPR1 antibody. Images were obtained using a ChemDoc XRS+ imaging system (Bio-Rad), lanes and bands were defined using Image Lab software (Bio-Rad), and the bands corresponding to NPR1 proteins were quantified based on the signal intensity relative to time 0. In planta degradation assays were performed as previously described[27], except that endogenous NPR1 levels were monitored and seedlings were pre-treated with 0.1 mM or 1 mM SA. Western blotting and data analysis were performed as described for the cell-free degradation assays.

Phylogenetic analysis

For alignment of the C-terminal domains of NPR orthologues, the sequences of representative proteins were obtained from the Pfam database and aligned using Clustal Omega with default settings[28]. A neighbour-joining tree was created using the Phylogeny.fr web application[29] along with the iTOL software[30].

Statistics and reproducibility

In all statistical data, the centre values are the mean and the error bars represent standard deviation from the mean. No statistical methods were used to predetermine sample size. All experiments, except HDX-MS (once) and data associated with Extended Data Fig. 6a (twice), have been repeated three times or more with similar results.

Reporting summary

Further information on research design is available in the Nature Research Reporting Summary linked to this paper.

Data availability

Uncropped gels and DNA sequencing results of all constructs are included in Supplementary Data. Structural coordinates and structural factors have been deposited in the Protein Data Bank under accession number 6WPG. All reagents are available from the corresponding authors upon request. Source data are provided with this paper.

Code availability

All software used in this study is publicly available. These include HKL-2000 v.720 package, GraphPad Prism 7.00 and 8, Phenix 1.14-3260, Protein Prospector v.5.23.1, Microsoft Excel 2018, Clustal Omega and R Studio v.1.3.1225 with a script listed in Reporting Summary.

20. Hsu, P. L. et al. Crystal structure of the COMPASS H3K4 methyltransferase catalytic module. *Cell* **174**, 1106–1116.e9 (2018).
21. Otwinowski, Z. & Minor, W. Processing of X-ray diffraction data collected in oscillation mode. *Methods Enzymol*. **276**, 307–326 (1997).
22. Adams, P. D. et al. PHENIX: a comprehensive Python-based system for macromolecular structure solution. *Acta Crystallogr. D* **66**, 213–221 (2010).
23. Emsley, P., Lohkamp, B., Scott, W. G. & Cowtan, K. Features and development of Coot. *Acta Crystallogr. D* **66**, 486–501 (2010).
24. Clough, S. J. & Bent, A. F. Floral dip: a simplified method for *Agrobacterium*-mediated transformation of *Arabidopsis thaliana*. *Plant J*. **16**, 735–743 (1998).
25. Pajerowska-Mukhtar, K. M. et al. The HSF-like transcription factor TBF1 is a major molecular switch for plant growth-to-defense transition. *Curr. Biol*. **22**, 103–112 (2012).
26. Bates, D., Machler, M., Bolker, B. M. & Walker, S. C. Fitting linear mixed-effects models using lme4. *J. Stat. Softw*. **67**, 1–48 (2015).
27. Skelly, M. J., Furniss, J. J., Grey, H., Wong, K. W. & Spoel, S. H. Dynamic ubiquitination determines transcriptional activity of the plant immune coactivator NPR1. *eLife* **8**, e47005 (2019).
28. Sievers, F. et al. Fast, scalable generation of high-quality protein multiple sequence alignments using Clustal Omega. *Mol. Syst. Biol*. **7**, 539 (2011).
29. Dereeper, A. et al. Phylogeny.fr: robust phylogenetic analysis for the non-specialist. *Nucleic Acids Res*. **36**, W465–W469 (2008).
30. Letunic, I. & Bork, P. Interactive tree of life (iTOL) v3: an online tool for the display and annotation of phylogenetic and other trees. *Nucleic Acids Res*. **44**, W242–W245 (2016).

Acknowledgements We thank the beamline staff at ALS for help with data collection; T. Sun and Y. Zhang for advice on optimizing the radiolabelled ligand binding assay for NPR1; members of the N.Z., X.D. and W. Xu laboratories for discussion and help; Z. Mou for an NPR1 antibody; Y. Tada for the wheat-germ-based in vitro translation system; M. Mwimba for help with statistical analysis; and C. Sponsel for assisting with nucleic acid preparations for quantitative PCR and screening transgenic lines. This work is supported by the Howard Hughes Medical Institute to N.Z. and X.D., the Gordon and Betty Moore Foundation (GBMF3032) and the National Institutes of Health (2R01-GM069594-09 and 5R35-GM118036) to X.D., Henan University to W.W., an NRSA fellowship from NIGMS (1F32-GM122250-01A1) to P.J.Z., and Duke University Department of Biology Hargitt postdoctoral research fellowships to J.W. and P.J.Z.

Author contributions W.W., J.W., H.L., S.Y., X.D. and N.Z. conceived the project. H.L. designed, and H.L. and W.W. performed, the proteolytic mapping experiments. H.L. determined the SBC of NPR4. H.L., D.-V.R. and H.S. tested different constructs for protein purification and crystallization. H.L. and W.W. obtained the diffracting crystals. W.W. and N.Z. determined and analysed the structures. J.W. created NPR4 point mutations, carried out all in planta experiments, performed the majority of the domain swaps, and conducted most of the radiolabelled SA ligand binding assays, with the exception of the NPR1 SA-binding curves, which were conducted by T.R.H. M.G. and W.W. conducted the HDX experiments and analysed the data. P.J.Z. performed the NPR1 degradation assays and phylogenetic analysis of NPR proteins for selected land plants, L.L. contributed constructs for the NPR1–NPR4 domain swaps, S.Y. conducted the initial SA-binding assays for the NPR1–NPR4 domain swaps, W.W., J.W., P.J.Z., X.D. and N.Z. wrote the manuscript with help from all of the co-authors.

Competing interests N.Z. is a cofounder of Coho Therapeutics and a Scientific Advisory Board member of Kymera Therapeutics. X.D. is a cofounder of Upstream Biotechnology, Inc., and a Scientific Advisory Board member of Inari Agriculture.

Additional information

Supplementary information is available for this paper at https://doi.org/10.1038/s41586-020-2596-y.

Correspondence and requests for materials should be addressed to X.D. or N.Z.

Peer review information *Nature* thanks John Burke, Steven Spoel and the other, anonymous, reviewer(s) for their contribution to the peer review of this work.

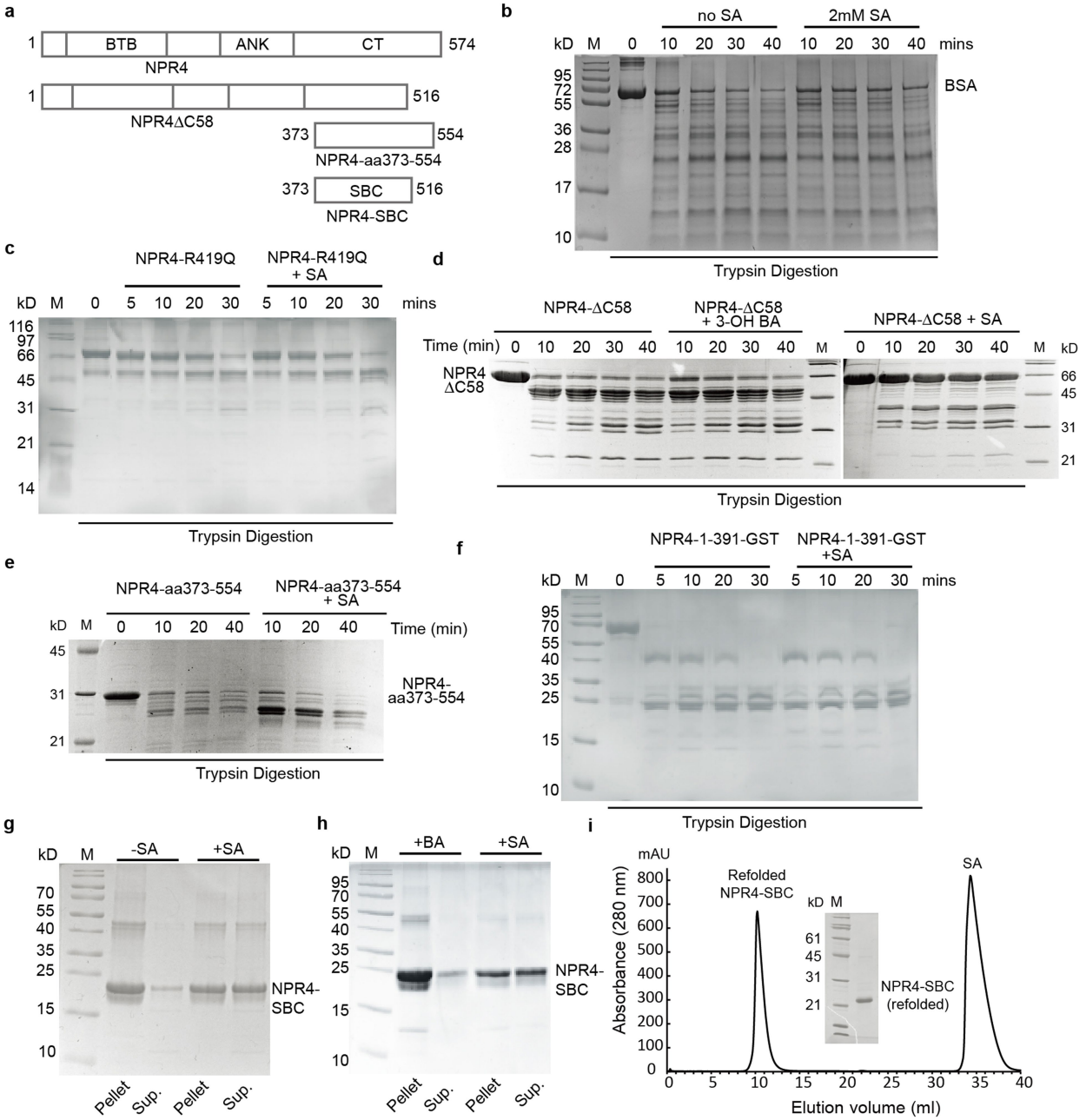

Extended Data Fig. 1 | Mapping and refolding of the NPR4 SBC. Related to Figs. 1, 2. **a**, Domain arrangements of *A. thaliana* NPR4 and different constructs used for mapping NPR4 SBC. **b**–**f**, Comparison of trypsin digestion profiles of truncated NPR4 proteins with or without 1 mM SA or 3-OH BA. Negative controls of limited proteolytic digestion of NPR4 were conducted with bovine serum albumin (BSA) (**b**), SA-insensitive NPR4(R419Q) mutant associated with *npr4-4D* (**c**) and NPR4(1–391) fragment (**f**). **g**, **h**, SA-dependent refolding of NPR4 SBC polypeptide affects its solubility. BA, benzoic acid, an inactive analogue of SA; Sup., supernatant; M, molecular weight marker. **i**, Superdex 75 size exclusion chromatography elution profile of the NPR4 SBC fragment refolded in the presence of SA. Excess SA was eluted after one column volume owing to a weak interaction with the resin. The inset shows the final purified NPR4 SBC fragment analysed by SDS–PAGE with Coomassie staining. Experiments in **b**–**i** were repeated three times or more with similar results.

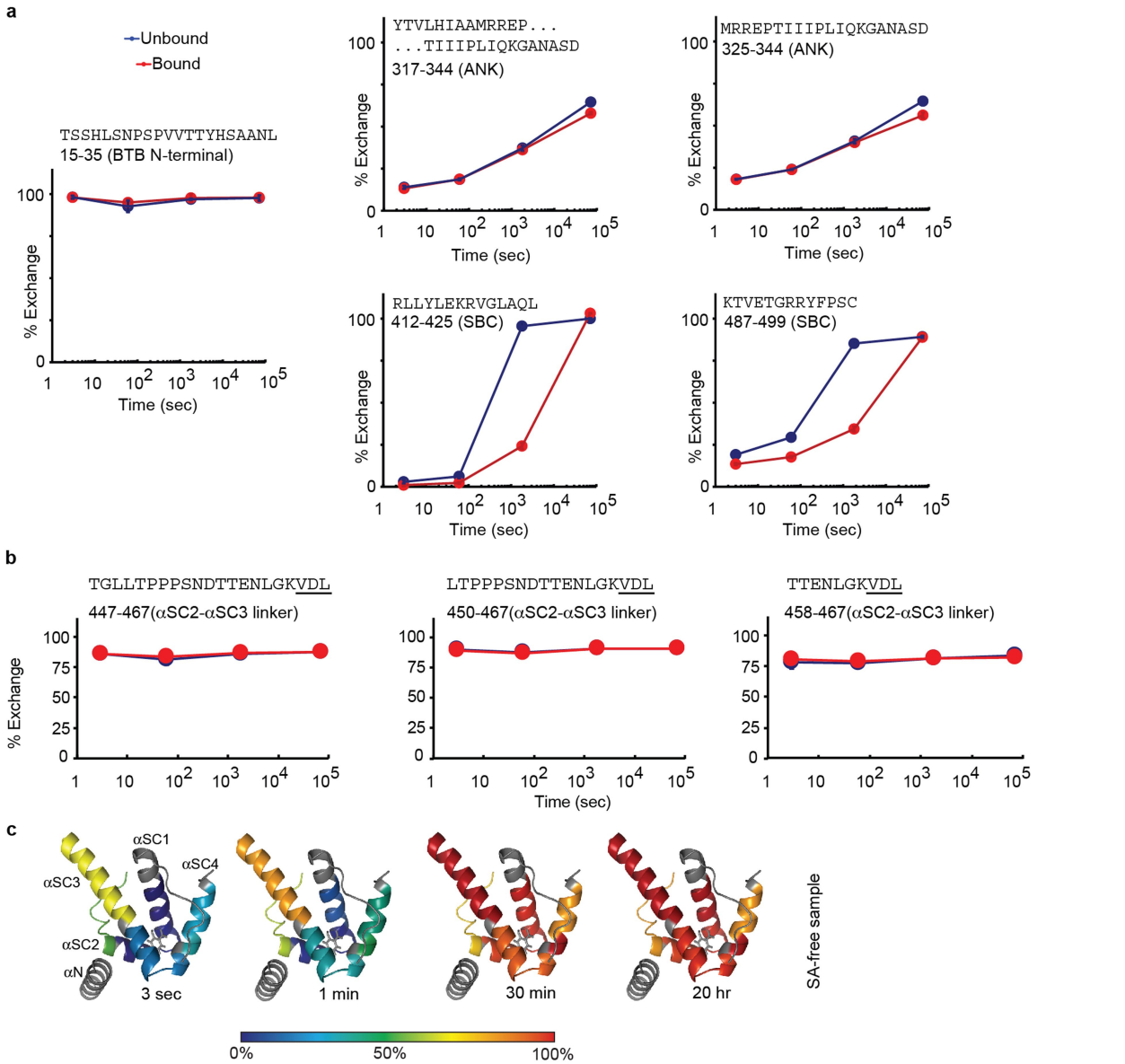

Extended Data Fig. 2 | Deuterium exchange profiles of selected NPR4 peptides. Related to Fig. 2. **a**, Deuterium uptake plots of representative peptides of NPR4 SBC derived from samples with (red) or without (blue) the presence of 0.1 mM SA. The SA-insensitive deuterium uptake plots of a BTB domain N-terminal peptide are shown on the left as a representative SA-insensitive region. $n = 3$ independent samples. Error bars representing s.d. (centre value) are shown, but are often too small to be seen. The peptide sequences, amino acid numbers and structural domain to which they belong are indicated on top of the plots. **b**, The SA-insensitive deuterium uptake plots of three peptides containing residues that belong to the proposed ethylene-responsive element-binding-factor-associated amphipathic repression (EAR) motif (underlined). **c**, The SA-free HDX profile is mapped on the NPR4 SBC crystal structure for the four time points, with a colour ramp scheme indicative of the percentage of exchange. Regions coloured in grey were outside of the peptide coverage.

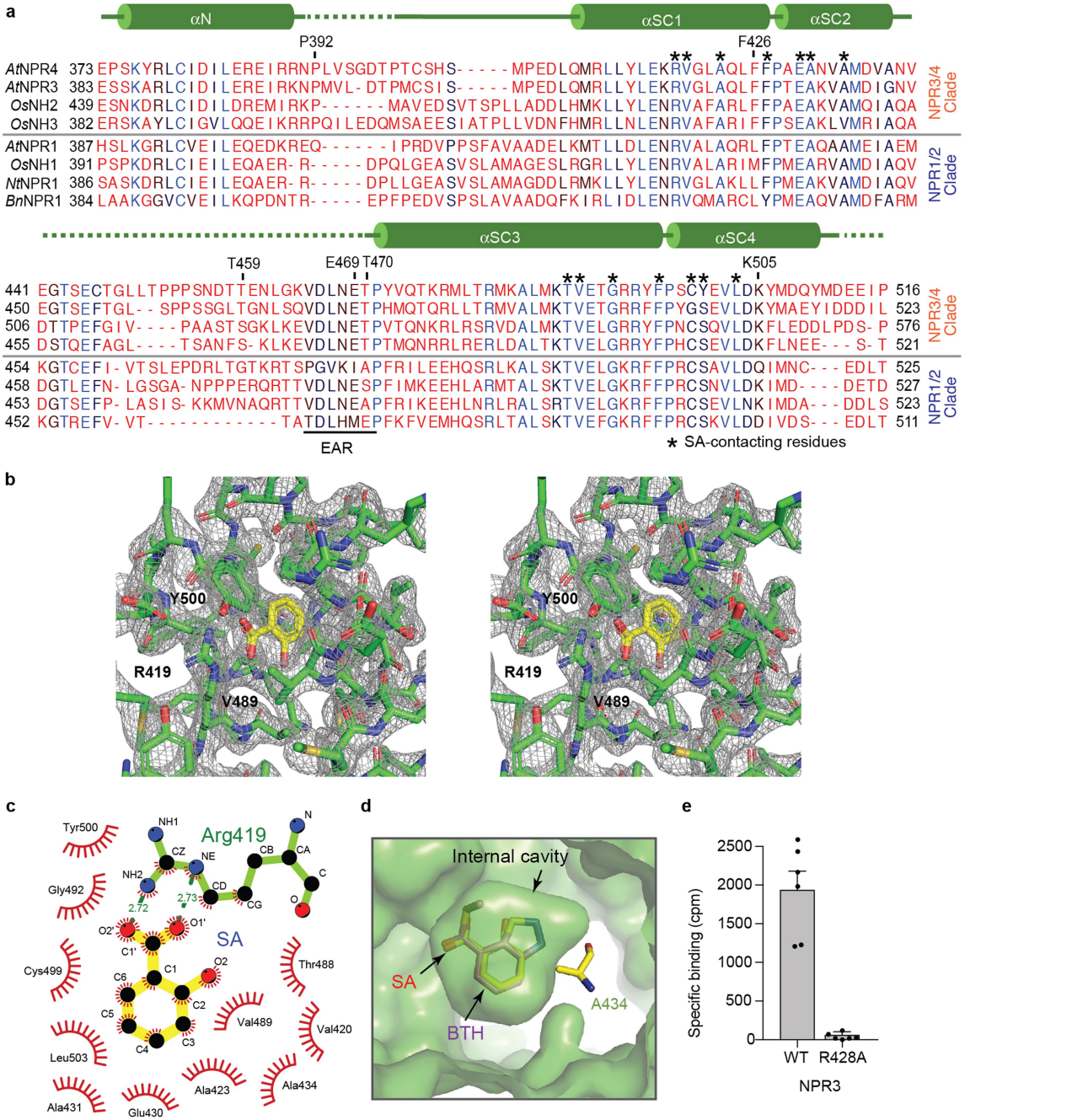

Extended Data Fig. 3 | Sequence alignment of the SBC regions in NPR proteins from several plant species, and details of the SA-binding pocket and activity. Related to Fig. 2. **a**, Structure-based sequence alignment of the SBC regions of NPR4 and NPR1 orthologues. The secondary-structure diagram of NPR4 SBC is shown above the sequences. Regions with no regular secondary structure are shown by lines, and α-helices are represented by cylinders. The dashed lines indicate two disordered loops that are not resolved in the structure. Strictly conserved residues are coloured in blue. The rest of the residues are coloured with black (87.5%), brown (75%) or red (<75%) based on their degrees of conservation. The residues directly involved in SA binding are highlighted with asterisks. The putative EAR motif is labelled and indicated by a black bar. Six surface residues selected for mutagenesis analysis are labelled. *At* (*Arabidopsis thaliana*): *NPR1* AT1G64280, *NPR3* AT5G45110 and *NPR4* AT4G19660) *Os* (*Oryza sativa*): *NH1* Os01g09800, *NH2* Os01g56200 and *NH3* Os03g46440; *Nb* (*Nicotiana benthamiana*): *NPR1* LOC107831756; *Bn* (*Brassica napa*) *NPR1* LOC106389246. **b**, A close-up stereo view of the NPR4 SBC SA-binding pocket with the omit map electron density, shown together with the residues in the stick model. SA is coloured in yellow and red and situated in the centre. Three selected SA-contacting residues in close proximity to the SA carboxyl group are indicated. **c**, Ligplot of the hydrophobic and polar interactions between SA and NPR4-SBC residues. **d**, A semi-transparent view of the SA-binding pocket with the SA analogue benzothiadiazole (BTH) (magenta, blue and red sticks) modelled onto SA (yellow and red sticks) situated in the centre and indicated by arrows. The view is related to the NPR4 SBC internal cavity shown in Fig. 2c by 180° vertical rotation. Ala434 is shown as a yellow stick, and indicated as A434. The internal cavity and surrounding surfaces of NPR4 SBC are shown in green surface representation. **e**, SA binding by wild-type NPR3 (WT) and NPR3(R428A) as determined with radiolabelled ligand binding assay with 100 nM ^{3}H-SA. $n = 6$ independent samples. Error bars indicate s.d. (centre value).

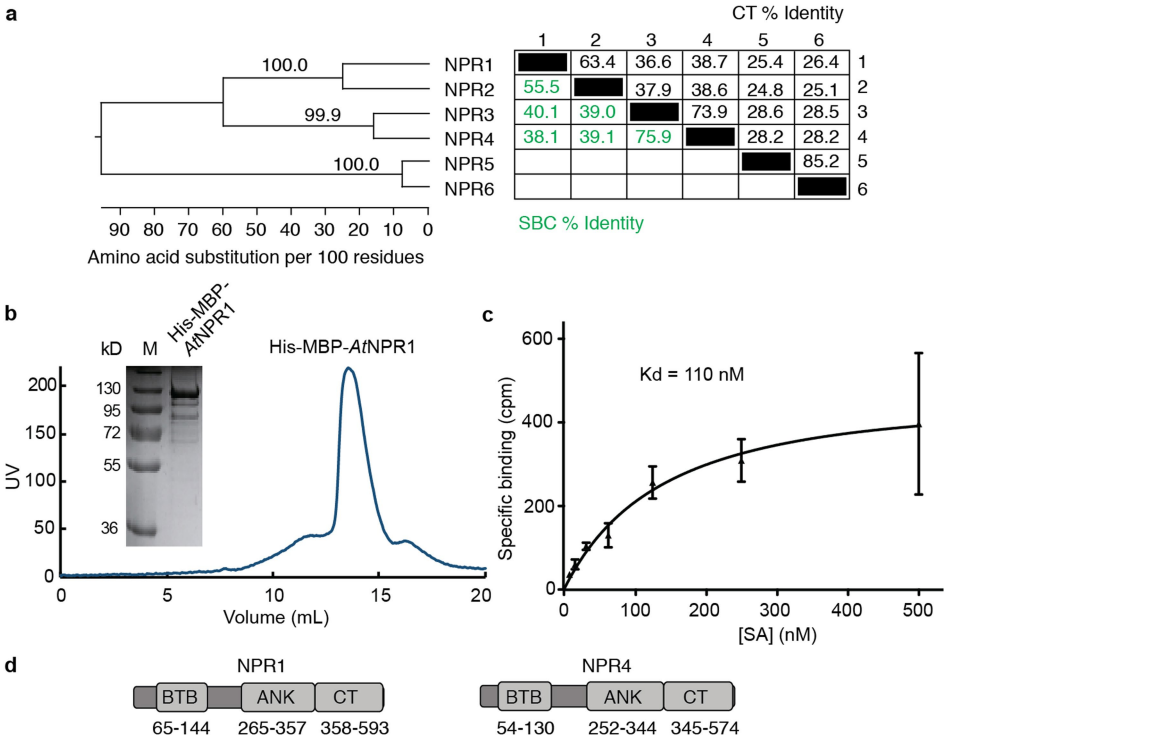

Extended Data Fig. 4 | Sequence comparison of *Arabidopsis* NPRs and characterization of His–MBP–NPR1. Related to Fig. 3. **a**, Neighbour-joining tree of NPR C-terminal (CT) domains and pairwise comparisons of amino acid sequence identity within the CT and SBC regions. Bootstrap values are noted for the branching of each node. Numbers 1–6 correspond to the six *Arabidopsis* NPRs. Despite featuring similar CT regions, NPR5 and NPR6 do not contain a regular SBC, reflected by the low sequence identity of their CT domains to that of NPR1, NPR2, NPR3 and NPR4. **b**, Size-exclusion chromatography elution profile of His–MBP–NPR1, which was first purified by amylose affinity chromatography. The inset shows the final purified His–MBP–NPR1 protein analysed by SDS–PAGE with Coomassie staining. Experiments were repeated three times with similar results. **c**, Dose–response curve of SA binding by NPR1. In the radiolabelled ligand binding assay, 5 μg of His–MBP–NPR1 protein was incubated with ^{3}H-SA at different concentrations. Three replicates in a single experiment were used to calculate the K_d of SA binding to NPR1. $n = 3$ independent samples. Error bars represent s.e.m. (centre value). cpm, counts per minute. **d**, Diagrams of NPR1 and NPR4 domain boundaries that are relevant to Fig. 3d.

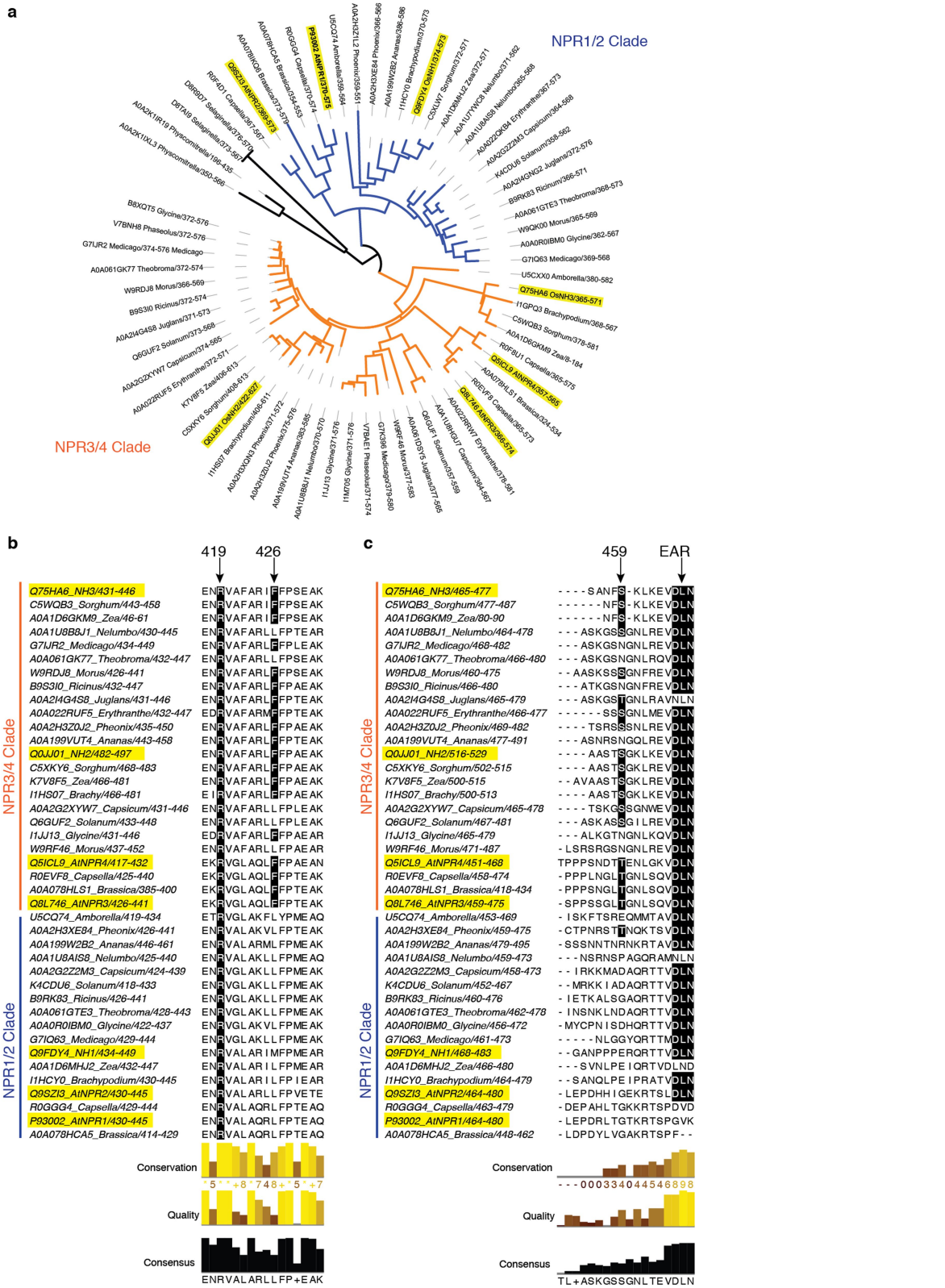

Extended Data Fig. 5 | NPR amino acid sequence homology in angiosperms. Related to Fig. 3. **a**, Neighbour-joining tree depicting the divergence of the CT domains of *A. thaliana* NPRs and *O. sativa* NH proteins (highlighted), as well as relationship with other NPR-like proteins in angiosperms. Black, out groups; blue, NPR1 and NPR2 clade; and orange, NPR3 and NPR4 clade. **b**, **c**, Amino acid sequence alignments of NPR C terminal domains indicating the amino acid conservation (black shade) at the position (arrow) of NPR4 residues R419 and F426 (**b**), as well as T459 and the putative EAR motif (**c**). The degree of conservation, alignment quality and conservation strength are indicated by the histograms below the sequences.

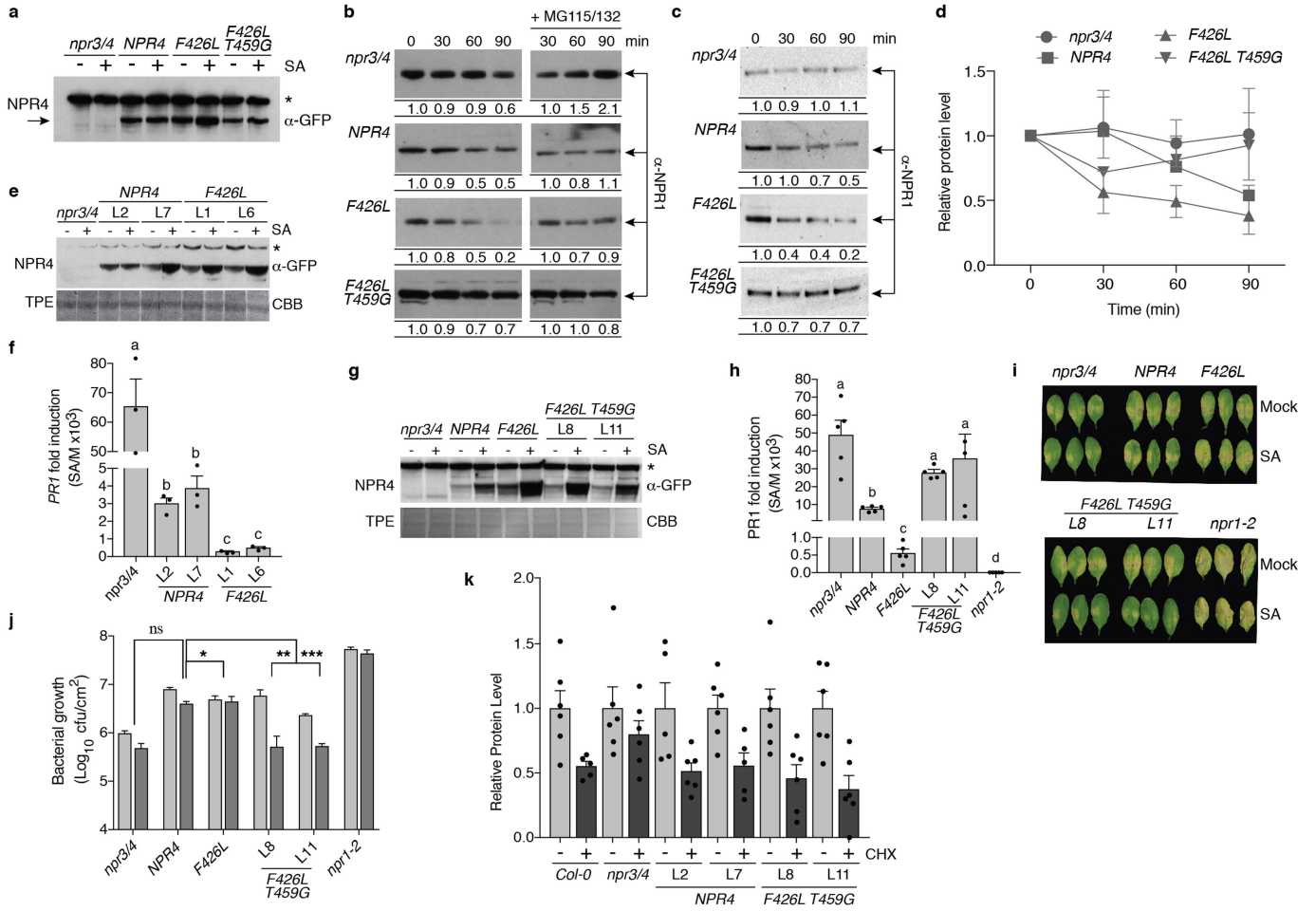

Extended Data Fig. 6 | NPR4-point-mutant expression and their differential phenotypic effects. Related to Fig. 4. **a**, Western blot analysis of transgenic *npr3 npr4* (*npr3/4*) seedlings expressing similar amounts of the NPR4–GFP variants 24 h after treatment with 0.1 mM SA. An antibody against GFP (anti-GFP) was used. Asterisk denotes a nonspecific band. Experiments were repeated two times with similar results. **b**, Western blot depicting cell-free protein-degradation assays comparing the rate of endogenous NPR1 degradation in protein extracts from **a**; quantifications of the data are shown in Fig. 4a. Arrows, endogenous NPR1; MG115/132, proteasome inhibitors. The ratios listed below each sample indicate NPR1 levels compared to 0 min for the degradation assay or 30 min for samples containing MG115/132. An antibody against NPR1 (anti-NPR1) was used. Experiments were repeated three times with similar results. **c**, **d**, In planta protein-degradation assays comparing the rate of endogenous NPR1 degradation in seedlings pretreated with 0.1 mM SA for 24 h. NPR1 was detected using an anti-NPR1 antibody (**c**) and the relative band intensities were quantified (**d**). $n = 3$ independent biological samples. Error bars indicate s.d. (centre values). **e**, Western blot analysis of transgenic *npr3 npr4* seedlings expressing NPR4–GFP or NPR4(F426L)–GFP after a 24-h treatment with 0.1 mM SA. L1, L2, L6 and L7, independent transgenic lines; TPE, total protein extract; CBB, Coomassie brilliant blue. An antibody against GFP (anti-GFP) was used. Asterisks denotes a non-specific band. **f**, Fold change of *PR1* expression in seedlings from **e** 24 h after 0.1 mM SA treatments. The data are normalized to *UBQ5* expression, error bars indicate s.d. ($n = 3$). Statistical significance was determined by one-way ANOVA on log-transformed data, followed by Tukey's multiple comparison correction; letters indicate statistical significance, $P < 0.05$. **g**, Western blot analysis of mature leaves from transgenic *npr3 npr4* plants expressing NPR4–GFP, NPR4(F426L)–GFP or NPR4(F426L/T459G)–GFP after a 6-h treatment with 0.5 mM SA spray. L8 and L11 denote independent transgenic lines. An antibody against GFP (anti-GFP) was used. Asterisk denotes a non-specific band. **h**, Fold change of *PR1* expression in leaves from **g** 6 h after mock or 0.5 mM SA spray. The data are normalized to *UBQ5* expression. $n = 5$ biologically independent samples. Error bars indicate s.d. (centre values). Statistical significance was determined by one-way ANOVA on log-transformed data, followed by Tukey's multiple comparison correction; letters indicate statistical significance, $P < 0.05$. **i**, **j**, SA protection against *P. syringae* pv. *maculicola* ES4326 infection. Images of the development of disease symptoms (**i**) and bacterial growth in infected leaves (**j**) were recorded 3 d after inoculation at $OD_{600\,nm} = 0.001$. Light grey bars, mock; dark grey bars, 0.1 mM SA. Colony-forming units (cfu) were determined for three experiments and combined using linear mixed effect model (lme4) with experiment as random effects. $n = 3$ experiments each with 8 biological repeats per genotype and treatment. Error bars indicate s.d. (centre value). Statistical significance was determined by two-way ANOVA on log-transformed data. NS $P = 0.6$, $^{*}P = 0.03$; $^{**}P = 0.008$; $^{***}P = 0.0004$. Experiments in **i** were repeated three times with similar results. **k**, Relative band intensities were quantified after in planta protein degradation assays comparing the rate of endogenous NPR1 degradation in seedlings pretreated with 1 mM SA for 24 h as in **c**, **d**. $n = 5$ biologically independent samples. Error bars indicate s.e.m. (centre values).

Extended Data Table 1 | Crystallography data collection and refinement statistics

	Native	Pt-NPR4-SBC-derivative
Data collection		
Space group	$P3_121$	$P3_121$
Cell dimensions		
a, *b*, *c* (Å)	88.293, 88.293, 138.003	88.219, 88.219, 138.034
α, β, γ (°)	90, 90, 120	90, 90, 120
		Peak
Wavelength (Å)		1.072
Resolution (Å)	2.28	2.80
R_{merge}	0.064 (0.771)	0.105 (0.673)
$I / \sigma I$	23.3 (2.8)	15.2 (2.6)
Completeness (%)	99.31 (96.44)	99.8 (99.7)
Redundancy	10.6 (8.4)	6.4 (6.2)
Refinement		
Resolution (Å)	2.28	
No. reflections	28714 (2733)	
R_{work} / R_{free}	0.205/0.224	
No. atoms		
Protein	1855	
Ligand/ion	20/0	
Water	76	
B-factors	79.68	
Protein	79.85	
Ligand/ion	55.16	
Water	82.16	
R.m.s deviations		
Bond lengths (Å)	0.009	
Bond angles (°)	0.878	

This table describes the data collection, phasing and refinement statistics of His–NPR4 SBC crystals. Values in parentheses are for highest-resolution shell.

nature research

Corresponding author(s): Ning Zheng, Xinnian Dong

Last updated by author(s): 05/06/2020

Reporting Summary

Nature Research wishes to improve the reproducibility of the work that we publish. This form provides structure for consistency and transparency in reporting. For further information on Nature Research policies, see Authors & Referees and the Editorial Policy Checklist .

Statistics

For all statistical analyses, confirm that the following items are present in the figure legend, table legend, main text, or Methods section.

n/a	Confirmed
☐	☒ The exact sample size (*n*) for each experimental group/condition, given as a discrete number and unit of measurement
☐	☒ A statement on whether measurements were taken from distinct samples or whether the same sample was measured repeatedly
☐	☒ The statistical test(s) used AND whether they are one- or two-sided *Only common tests should be described solely by name; describe more complex techniques in the Methods section.*
☐	☒ A description of all covariates tested
☐	☒ A description of any assumptions or corrections, such as tests of normality and adjustment for multiple comparisons
☐	☒ A full description of the statistical parameters including central tendency (e.g. means) or other basic estimates (e.g. regression coefficient) AND variation (e.g. standard deviation) or associated estimates of uncertainty (e.g. confidence intervals)
☒	☐ For null hypothesis testing, the test statistic (e.g. *F*, *t*, *r*) with confidence intervals, effect sizes, degrees of freedom and *P* value noted *Give P values as exact values whenever suitable.*
☒	☐ For Bayesian analysis, information on the choice of priors and Markov chain Monte Carlo settings
☒	☐ For hierarchical and complex designs, identification of the appropriate level for tests and full reporting of outcomes
☒	☐ Estimates of effect sizes (e.g. Cohen's *d*, Pearson's *r*), indicating how they were calculated

Our web collection on statistics for biologists contains articles on many of the points above.

Software and code

Policy information about availability of computer code

Data collection

Our crystal reflection data were indexed, integrated and scaled with the HKL-2000 v720 package.

Data analysis

Prism 7.00 was used to analyze and produce graphs.
The SAD method was used to determine the initial phase using PHENIX 1.14-3260. Initial structural models were built, refined using COOT 0.8.9 and PHENIX 1.14-3260.

In the HDX experiments, the peptides were identified using Protein Prospector V5.23.1.

Microsoft Excel 2018
GraphPad Prism Version 8
BioRad ImageLab Version 6.0.1 build 34 Standard Edition

Where indicated (Extended Data Fig. 6j) statistical analysis was conducted using R Studio V1.3.1225 with the following code:

```
library(lme4 V1.1-23)
JW<- read.csv("JWither.csv",header = TRUE)
attach(JW)
temp<-JW[Genotype=="npr3/4",]

temp.mdl=lmer(Log10.cfu.cm2~Treatment+(1|Experiment), data = temp, REML=FALSE)
qqnorm(residuals(temp.mdl))
summary(temp.mdl)
```

temp<-JW[Genotype=="npr1-2",]
temp<-JW[Genotype=="4-7.2",]
temp<-JW[Genotype=="5-1.6",]
temp<-JW[Genotype=="12A8",]
temp<-JW[Genotype=="12A11",]
Sum of normal distributions
Cfu of three experiments (8 biological replicates each) were combined using linear mixed effect model (lme4) with experiment as random effects. Data are mean ± s.d ; t-test; *p < 0.05.
Citation: https://www.jstatsoft.org/article/view/v067i01

Phylogenetic analysis: For alignment of the C-terminal NPR domains, the sequences of representative domains were obtained from the Pfam database and were aligned using Clustal Omega with default settings (http://msb.embopress.org/content/7/1/539). A neighbour-joining tree was created using the Phylogeny.fr web application along with the iTOL software (cited in methods and references section)

For manuscripts utilizing custom algorithms or software that are central to the research but not yet described in published literature, software must be made available to editors/reviewers. We strongly encourage code deposition in a community repository (e.g. GitHub). See the Nature Research guidelines for submitting code & software for further information.

Data

Policy information about availability of data

All manuscripts must include a data availability statement. This statement should provide the following information, where applicable:

- Accession codes, unique identifiers, or web links for publicly available datasets
- A list of figures that have associated raw data
- A description of any restrictions on data availability

All data are available in the main text or supplementary materials. For material requests, please contact the corresponding author. The protein coordinate and atomic structure factors have been deposited in the Protein Data Bank (PDB) and are available with accession codes 6WPG.

Field-specific reporting

Please select the one below that is the best fit for your research. If you are not sure, read the appropriate sections before making your selection.

☒ Life sciences ☐ Behavioural & social sciences ☐ Ecological, evolutionary & environmental sciences

For a reference copy of the document with all sections, see nature.com/documents/nr-reporting-summary-flat.pdf

Life sciences study design

All studies must disclose on these points even when the disclosure is negative.

Sample size	No sample size calculation was done for the in vitro and in vivo studies described in this manuscript. The sample sizes chosen were based on our previous studies for reproducibility and widely adopted protocols in the field.
Data exclusions	No data were excluded from the analyses
Replication	All experiments were repeated at least two times, most experiments were repeated at least three times. Each time the results were repeatable.
Randomization	Samples of the same genotypes or same developmental stages were randomly collected. They are subsequently allocated into experimental groups for comparison of genotype effects.
Blinding	Experiments were not blinded because of the need for selection of appropriate developmental stage for treatments and sample collections.

Reporting for specific materials, systems and methods

We require information from authors about some types of materials, experimental systems and methods used in many studies. Here, indicate whether each material, system or method listed is relevant to your study. If you are not sure if a list item applies to your research, read the appropriate section before selecting a response.

Materials & experimental systems

n/a	Involved in the study
[ ]	[x] Antibodies
[ ]	[x] Eukaryotic cell lines
[x]	[ ] Palaeontology
[x]	[ ] Animals and other organisms
[x]	[ ] Human research participants
[x]	[ ] Clinical data

Methods

n/a	Involved in the study
[x]	[ ] ChIP-seq
[x]	[ ] Flow cytometry
[x]	[ ] MRI-based neuroimaging

Antibodies

Antibodies used

anti-GFP: Takara Bio Clontech. Living Colors A.v. Mouse Monoclonal Antibody (JL-8) Catalog #: 632381; RRID:AB_2313808; Lot #: 070313 (Dilution = 1 ug/ul)

anti-NPR1: Developed as described by Mou et al. (Cell 113: 935-944), except that the N–terminus of NPR1 (nucleotides 1–1395) was cloned using NdeI and SalI into the NdeI and XhoI sites of pET23b (Novagen). Rabbit polyclonal anti-NPR1 antibody was developed and affinity-purified by Pierce/Thermo Fisher Scientific. (Dilution = 0.25 ug/ul)

anti-StrepII: EMD Millipore. Strep Tag II Antibody HRP Conjugate is a peroxidase-conjugated Strep•Tag II Monoclonal Antibody Catalog #: 71591-3. Lot#: 3045540 and Lot # 3275059 (Dilution = 0.5 ug/ul)

anti-GST: GE Healthcare. Antibody is a peroxidase conjugated GST Monoclonal Antibody Catalog #: RPN1236; RRID:AB_771429; Lot # 9845873 (Dilution = 0.5 ug/ul)

anti-HA: BioLegend. Anti-HA.11 Mouse Monoclonal Epitope Tag Antibody (Clone: 16B12). Catalog #: 901513 RRID:AB_2820200 (Dilution = 0.5 ug/ul)

anti-FLAG: Sigma-Aldrich. Mouse Monoclonal anti-FLAG M2 antibody. (Clone: M2) Catalog #: F1804; RRID:AB_262044; Lot # SLBN5629V (Dilution = 0.5 ug/ul)

Goat anti-Mouse IgG (H+L) Secondary Antibody, HRP. Thermo-Fisher Scientific. Catalog # 31430 RRID:AB_228307. (Dilution 0.15 ug/ul)
Goat anti-Rabbit IgG (H+L) Secondary Antibody, HRP. Thermo-Fisher Scientific. Catalog # 31460 RRID:AB_228341. (Dilution 0.08 ug/ul)

Validation

anti-GFP: Takara Bio Clontech; Living Colors A.v. Mouse Monoclonal Antibody (JL-8); Catalog #: 632381;
Validation and Certificate of Analysis: https://www.takarabio.com/assets/documents/Certificate%20of%20Analysis/632380-632381-070313.pdf

anti-NPR1: Validated for detection of Arabidopsis NPR1 as described by Mou et al. (Cell 113: 935-944). The specificity of the newly developed anti-NPR1 antibody was confirmed using the npr1–3 mutant (Cao et al., 1997) (Figure S12a).

anti-StrepII: EMD Millipore. Catalog #: 71591-3. Strep Tag II Antibody HRP Conjugate.
Used to detect StrepII tag fusion proteins produced in E. coli in this manuscript.
Product Information: http://www.emdmillipore.com/US/en/product/StrepTag-II-Antibody-HRP-C71591-3onjugate,EMD_BIO-71591#anchor_Description

anti-GST: GE Healthcare. Catalog #: RPN1236. Antibody is a peroxidase conjugated GST Monoclonal Antibody.
Product Information: https://www.sigmaaldrich.com/catalog/product/sigma/gerpn1236?lang=en&region=US

anti-HA: BioLegend. Catalog #: 901513. Anti-HA.11 Mouse Monoclonal Epitope Tag Antibody (Clone: 16B12).
Certificate of Analysis: https://www.biolegend.com/fr-fr/global-elements/pdf-popup/anti-ha-11-epitope-tag-antibody-11071?filename=Anti-HA11%20Epitope%20Tag%20Antibody.pdf&pdfgen=true

anti-FLAG: Sigma-Aldrich. Catalog #: F1804. Mouse Monoclonal anti-FLAG M2 antibody.
Certificate of Analysis: https://www.sigmaaldrich.com/catalog/CertOfAnalysisPage.do?symbol=F1804&LotNo=SLBW3851&brandTest=SIGMA&returnUrl=%2Fproduct%2FSIGMA%2FF1804

Goat anti-Mouse IgG (H+L) Secondary Antibody, HRP. Thermo-Fisher Scientific. Catalog # 31430. Product Information https://www.thermofisher.com/antibody/product/Goat-anti-Rabbit-IgG-H-L-Secondary-Antibody-Polyclonal/31460

Goat anti-Rabbit IgG (H+L) Secondary Antibody, HRP. Thermo-Fisher Scientific. Catalog # 31460. Product Information https://www.thermofisher.com/order/genome-database/generatePdf?productName=&assayType=PRANT&productId=31430

Eukaryotic cell lines

Policy information about cell lines

Cell line source(s)	Sf9 (from Life Technologies B825-01) and High Five (from Life Technologies B85502) insect cells were used for recombinant protein expressions only
Authentication	Cells have been authenticated by the vendors. No further authentication was performed for commercially available cell lines.
Mycoplasma contamination	Cells were not tested for mycoplasma contamination.
Commonly misidentified lines (See ICLAC register)	no commonly misidentified cell lines were used